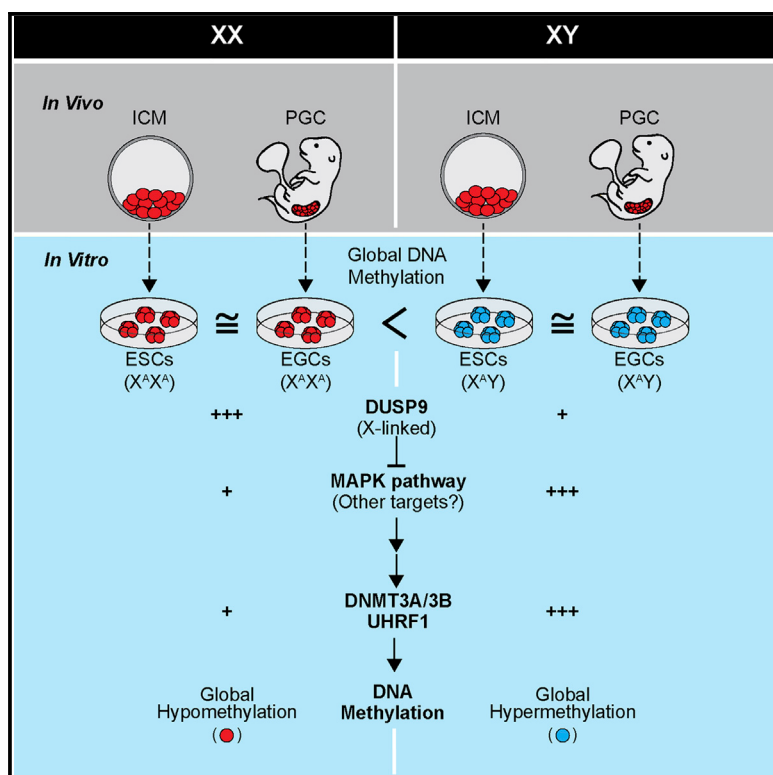


DUSP9 Modulates DNA Hypomethylation in Female Mouse Pluripotent Stem Cells

Graphical Abstract



Authors

Jiho Choi, Kendall Clement,
Aaron J. Huebner, ..., Steven P. Gygi,
Alexander Meissner,
Konrad Hochedlinger

Correspondence

alex@broadinstitute.org (A.M.),
khochedlinger@mgh.harvard.edu (K.H.)

In Brief

The molecular equivalence of ESCs and EGCs remains incompletely understood. Choi et al. show that ESCs and EGCs are highly similar and that sex rather than cell type drives the transcriptional and epigenetic differences observed between individual cell lines. Female-specific hypomethylation is partially due to upregulation of the X-linked MAPK phosphatase DUSP9.

Highlights

- Transcriptional and epigenetic patterns were compared between isogenic ESCs and EGCs
- DNA methylation levels correlate with the X chromosome-to-autosome ratio
- Male and female blastocysts exhibit similarly low methylation levels
- DUSP9 overexpression reduces, while *Dusp9* loss increases, methylation levels in ESCs

Data resources

GSE94481
GSE68733

DUSP9 Modulates DNA Hypomethylation in Female Mouse Pluripotent Stem Cells

Jiho Choi,^{1,2,3,8} Kendell Clement,^{2,3,4,8} Aaron J. Huebner,^{1,2,3} Jamie Webster,^{2,3,4} Christopher M. Rose,⁵ Justin Brumbaugh,^{1,2,3} Ryan M. Walsh,^{1,2,3} Soohyun Lee,⁶ Andrej Savol,¹ Jean-Pierre Etchegaray,¹ Hongcang Gu,⁴ Patrick Boyle,⁴ Ulrich Elling,⁷ Raul Mostoslavsky,¹ Ruslan Sadreyev,¹ Peter J. Park,⁶ Steven P. Gygi,⁵ Alexander Meissner,^{2,3,4,*} and Konrad Hochedlinger^{1,2,3,9,*}

¹Department of Molecular Biology, Cancer Center and Center for Regenerative Medicine, Massachusetts General Hospital, 185 Cambridge Street, Boston, MA 02114, USA

²Harvard Stem Cell Institute, 1350 Massachusetts Avenue, Cambridge, MA 02138, USA

³Department of Stem Cell and Regenerative Biology, Harvard University, Cambridge, MA 02138, USA

⁴Broad Institute of MIT and Harvard, Cambridge, MA 02142, USA

⁵Department of Cell Biology, Harvard Medical School, 240 Longwood Avenue, Boston, MA 02115, USA

⁶Department of Biomedical Informatics, Harvard Medical School, 10 Shattuck Street, Boston, MA 02115, USA

⁷Institute of Molecular Biotechnology of the Austrian Academy of Sciences (IMBA), Vienna Biocenter (VBC), 1030 Vienna, Austria

⁸Co-first author

⁹Lead Contact

*Correspondence: alex@broadinstitute.org (A.M.), khochedlinger@mgh.harvard.edu (K.H.)

<http://dx.doi.org/10.1016/j.stem.2017.03.002>

SUMMARY

Blastocyst-derived embryonic stem cells (ESCs) and gonad-derived embryonic germ cells (EGCs) represent two classic types of pluripotent cell lines, yet their molecular equivalence remains incompletely understood. Here, we compare genome-wide methylation patterns between isogenic ESC and EGC lines to define epigenetic similarities and differences. Surprisingly, we find that sex rather than cell type drives methylation patterns in ESCs and EGCs. Cell fusion experiments further reveal that the ratio of X chromosomes to autosomes dictates methylation levels, with female hybrids being hypomethylated and male hybrids being hypermethylated. We show that the X-linked MAPK phosphatase DUSP9 is upregulated in female compared to male ESCs, and its heterozygous loss in female ESCs leads to male-like methylation levels. However, male and female blastocysts are similarly hypomethylated, indicating that sex-specific methylation differences arise in culture. Collectively, our data demonstrate the epigenetic similarity of sex-matched ESCs and EGCs and identify DUSP9 as a regulator of female-specific hypomethylation.

INTRODUCTION

Pluripotent stem cell lines are typically derived from preimplantation embryos, yielding embryonic stem cells (ESCs), or from fetal germ cells, generating embryonic germ cells (EGCs) (Reik and Surani, 2015). Moreover, pluripotent stem cells can be produced from somatic cells upon forced expression of transcription factors, giving rise to induced pluripotent stem cells (iPSCs) (Takahashi and Yamanaka, 2006). Although ESCs, EGCs, and iPSCs

are thought to be transcriptionally highly similar, EGCs exhibit epigenetic differences that have been suggested to reflect their origin from fetal germ cells. For example, EGCs derived from late-stage (embryonic day [E] 11.5–E12.5) germ cells show DNA hypomethylation at imprinted and non-imprinted genes, which mirrors epigenetic patterns in the fetal germline (Hajkova et al., 2010; Labosky et al., 1994; Popp et al., 2010; Tada et al., 1997). Furthermore, classic cell-cell fusion experiments between EGCs and somatic cells demonstrated loss of methylation at repetitive elements and imprinted loci in hybrids, suggesting that EGCs harbor dominant demethylation activity (Tada et al., 1997). ESCs appear to lack this activity when fused to somatic cells (Tada et al., 2001). A subsequent study confirmed these findings and implicated TET1 in EGC-specific demethylation of imprinted genes in hybrids (Piccolo et al., 2013). However, a systematic comparison of global DNA methylation patterns among parental ESCs, EGCs, and resultant hybrids has not yet been performed.

Accumulating evidence suggests that culture conditions can dramatically alter DNA methylation patterns in pluripotent cell lines (Ficz et al., 2013; Habibi et al., 2013; Hackett et al., 2013; Leitch et al., 2013). Although ESC lines maintained in conventional culture media (serum/LIF [Leukemia inhibitory factor]) show normal methylation levels that globally resemble somatic tissues, exposure to both mitogen-activated protein kinase (MAPK) and GSK3 inhibitors in the presence of LIF (2i/LIF) triggers an up to 4-fold reduction of global methylation patterns and concomitant acquisition of a more naive pluripotent state (Ficz et al., 2013; Habibi et al., 2013; Leitch et al., 2013; Ying et al., 2008). 2i/LIF culture-induced demethylation reportedly involves direct transcriptional silencing of the de novo methyltransferase genes *Dnmt3a* and *Dnmt3b*, as well as transcriptional upregulation of the dioxygenase genes *Tet1* and *Tet2*, by the pluripotency regulators PRDM14 and NANOG, resulting in both passive and active demethylation of the genome within a few passages (Ficz et al., 2013; Habibi et al., 2013; Hackett et al., 2013; Yamaji et al., 2013). More recently, downregulation of the

DNMT1 cofactor UHFR1 was suggested to contribute to 2i/LIF-induced hypomethylation as well (von Meyenn et al., 2016).

In addition to culture conditions, the sex of ESC lines may influence methylation patterns. Female mouse ESC lines cultured in serum/LIF exhibit a reduction of global methylation levels and a decrease in imprinted gene methylation when compared to male ESCs (Habibi et al., 2013; Hackett et al., 2013; Ooi et al., 2010; Zvetkova et al., 2005). Hypomethylation in XX ESCs was directly linked to the presence of two active X (X^A) chromosomes and reduced expression levels of DNMT3A/B (Zvetkova et al., 2005) or DNMT3L (Ooi et al., 2010), because XO subclones regained DNMT3A/B expression and global methylation patterns, similar to XX somatic cells. More recently, Schulz et al. (2014) discovered that female ESCs grown in serum/LIF exhibit reduced MAPK and GSK3 signaling; elevated *Prdm14*, *Nanog*, and *Tet1/2* mRNA levels; and reduced *Dnmt3a/b* mRNA levels relative to male ESCs, indicating that the presence of two X^A chromosomes recapitulates certain phenotypes of ESCs maintained in a naive pluripotent state. However, the mechanisms and X-linked regulators underlying female-specific hypomethylation remain elusive.

Here, we revisit the previous observation that late-stage EGCs exhibit widespread DNA hypomethylation and dominant demethylation activity over ESCs with the goal of identifying possible mechanisms and mediators underlying this phenotype. Previous comparisons between ESC and EGC lines were limited by a small number of cell lines (Sharov et al., 2003), developmental stages of germ cells with a variable degree of epigenetic reprogramming (E8.5) (Leitch et al., 2013), and differences in genetic background (Sharova et al., 2007), sex (Hatano et al., 2005; Tada et al., 1997), or culture conditions (Hackett et al., 2013). We therefore derived multiple isogenic E3.5 ESC and E11.5–E12.5 EGC lines under equivalent growth conditions to compare (1) global transcription, (2) genome-wide DNA methylation, and (3) the ability to induce DNA demethylation in fusion hybrids.

RESULTS

Generation of Isogenic ESCs and EGCs

We crossed female 129S6 mice (abbreviated as 129) to male C57B6/6J mice (abbreviated as B6) carrying a constitutive G418 resistance gene to derive isogenic, 129xB6 F1 ESC and EGC lines. Specifically, ESC lines were established from the inner cell masses (ICMs) of E3.5 blastocysts, whereas EGC lines were produced from post-migratory primordial germ cells (PGCs) of E11.5 and E12.5 genital ridges (Figure 1A). We derived a total of six male and four female EGC lines and three male and three female ESC lines (Figure 1B). All cell lines were derived in 2i/LIF and maintained in serum/LIF on feeders. This modification allowed us to use equivalent culture conditions for ESCs and EGCs (Leitch et al., 2010), which is not feasible with classic derivation protocols.

ESC and EGC lines could be propagated over multiple passages while maintaining pluripotency-associated markers such as alkaline phosphatase (AP) activity and endogenous NANOG and SOX2 expression, documenting their self-renewal potential (Figure 1C). Moreover, both ESCs and EGCs gave rise to differentiated teratomas comprising structures from all three germ layers (Figure S1A) and supported the development of coat-color

chimeras, demonstrating their pluripotency (Figures S1B and S1C). Critically, EGC lines, but not ESC lines, exhibited demethylation of the *Peg3* locus, implying successful erasure of genomic imprints, which is a hallmark of late-stage germ cells and derivative EGCs (Figure S1D). Consistent with this observation, EGCs contributed to neonatal and adult chimeras less efficiently than ESCs (Figure S1B). Altogether, these results show that our newly derived ESC and EGC lines exhibit the expected growth behavior, pluripotency marker profiles, imprinting patterns, and developmental potential.

Global Methylation Analysis Distinguishes ESCs and EGCs by Sex Rather Than Cell Type

To assess global methylation patterns in ESC and EGC lines, we first performed Southern blot analysis for repetitive elements and dot blot analysis for 5mC. We observed that both male ESC and EGC lines displayed a normally methylated genomic landscape while both female ESC and EGC lines were globally hypomethylated, suggesting that sex rather than cell type of origin is the main driver behind overall DNA methylation levels in these pluripotent cell lines (Figures S1E and S1F). To corroborate this result, we analyzed all cell lines by reduced representation bisulfite sequencing (RRBS), which measures methylation patterns at single-base resolution across the genome (Meissner et al., 2008). RRBS analysis confirmed these results, demonstrating that male ESC and EGC lines are globally hypermethylated relative to female ESC and EGC lines (Figure 1D). Accordingly, unsupervised hierarchical clustering separated these cell lines based on sex rather than cell type (Figure 1E). However, we noticed one exception: the female EGC line J-27 was normally methylated and clustered with male ESC and EGC lines (Figures 1D and 1E). Interphase fluorescence *in situ* hybridization (FISH) of this cell line using an X chromosome-specific probe showed that more than 90% of cells were XO, explaining the elevated methylation levels (Figure S1G) (Zvetkova et al., 2005). Other male or female ESC and EGC cultures contained predominantly cells with one or two X chromosomes, respectively. We conclude, based on examining global DNA methylation patterns by three independent assays, that our genetically matched ESC and EGC lines maintained in serum/LIF are distinguished by sex rather than cell type of origin.

Hypomethylation in XX ESCs and EGCs Occurs Evenly across Most Genomic Features

Although total DNA methylation levels were equivalent between ESCs and EGCs of the same sex, local distribution of methylation patterns could differ in the two cell types, as exemplified by demethylation of the *Peg3* locus exclusively in EGCs (Figure S1D). We therefore compared methylation patterns by RRBS across several genomic features for both autosomes and X chromosomes in ESCs and EGCs. This analysis confirmed that female ESC and EGC lines are similarly hypomethylated compared to male ESC and EGC lines at promoter regions (CpG islands and shores) and repetitive elements: long interspersed nuclear elements (LINEs), short interspersed nuclear elements (SINEs), and long terminal repeats (LTRs) (Figures S2A and S2B). Specifically, we found that 1,516 autosomal and 63 X-linked promoters were less methylated in female ESCs and EGCs (Figures S2C and S2D). Moreover, female-specific methylation patterns at

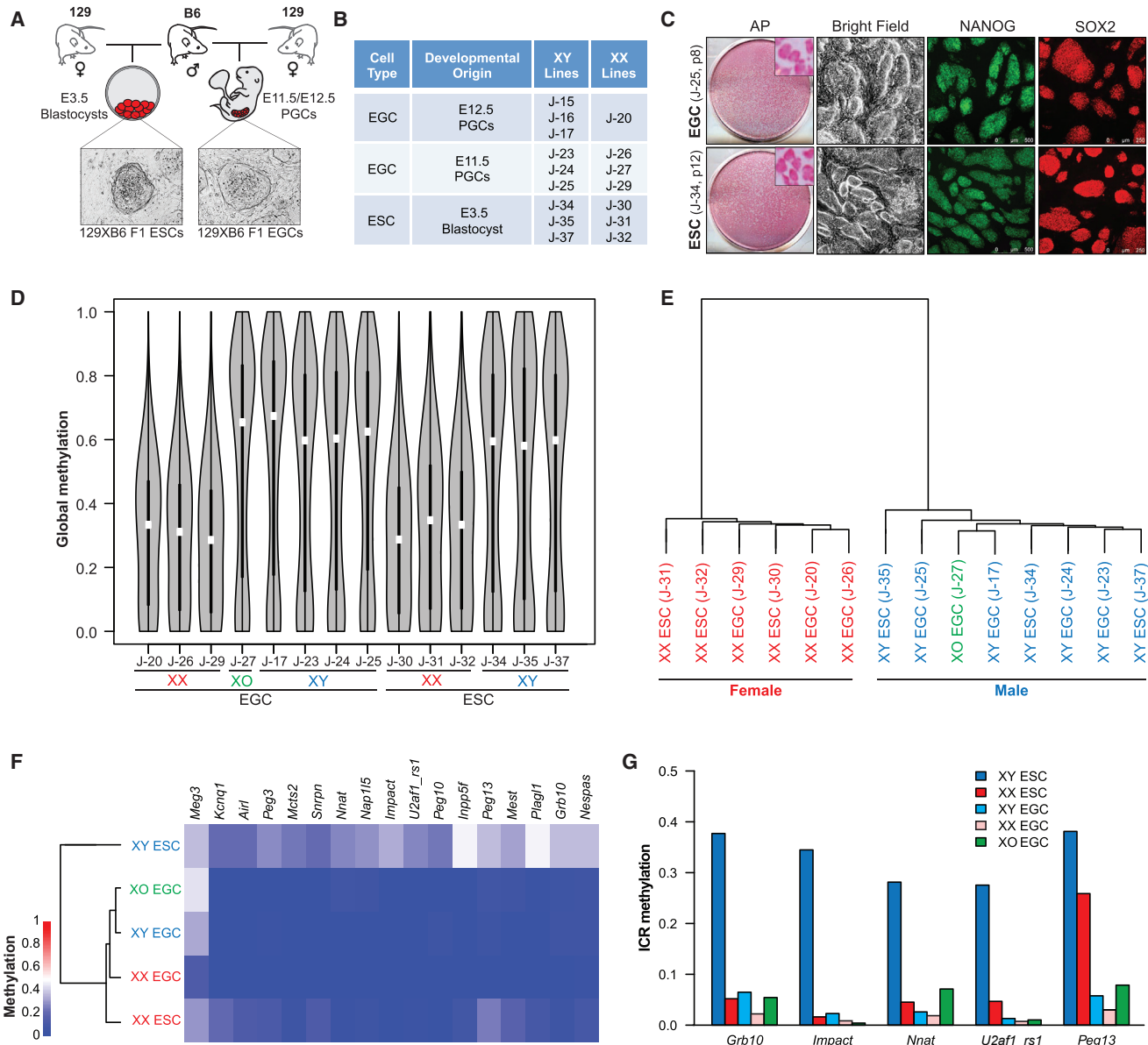


Figure 1. Sex, Rather Than Cell Type, Drives Global DNA Methylation Patterns in Pluripotent Cell Lines

(A) Schematic of the generation of genetically matched ESCs and EGCs.

(B) Detailed information on the established ESCs and EGCs. ESCs and EGCs were collected between passages 4 and 6 for all experiments unless otherwise specified.

(C) EGCs (top) and ESCs (bottom) express alkaline phosphatase (AP), NANOG, and SOX2. Insets show magnification of AP⁺ colonies.

(D) Global methylation analysis of isogenic ESC and EGC lines by reduced representation bisulfite sequencing (RRBS) using violin plot representations. White boxes indicate median methylation levels. Blue represents XY cells, red represents XX cells, and green represents the XO cell line.

(E) Unsupervised hierarchical clustering of RRBS samples shown in (D). Blue represents XY cells, red represents XX cells, and green represents the XO cell line.

(F) Dendrogram and heatmap representation of imprinted loci in isogenic ESC (n = 6) and EGC (n = 8) lines.

(G) Average methylation levels across imprinting control regions (ICRs) at indicated loci. Average values of methylation levels for three XY ESCs (dark blue), three XX ESCs (dark red), four XY EGCs (light blue), three XX EGCs (light red), and one XO EGC (green) line are shown for each gene.

See also Figures S1 and S2.

these promoter elements were more similar to those of a late-passage male *Dnmt3a/b* double-knockout (DKO) ESC line (Liao et al., 2015) than to a male wild-type ESC line (Figures S2C–S2E).

In contrast to methylation patterns across promoters and repetitive elements, CpGs associated with imprinting control regions (ICRs) showed notable cell type and sex-dependent differences. For example, ICR methylation was generally absent or

extremely low in EGC lines compared to male ESC lines, as expected (e.g., *Peg13*, *U2af1_rs1*, and *Snrpn*) (Figures 1F and 1G). However, female ESCs exhibited EGC-like hypomethylation at many ICR elements (e.g., *Grb10*, *Impact*, and *Nnat*), confirming epigenetic similarities between EGC lines and female ESC lines (Figures 1F and 1G) (Hackett et al., 2013). In accordance, unsupervised hierarchical clustering of samples based on all captured imprinted genes grouped female ESCs with male and female EGCs but separately from male ESCs (Figure 1F). Collectively, these results show that except for a few imprinted genes, such as *Meg3*, *Peg3*, and *Peg13* (Figures 1F and 1G; Figure S1D), hypomethylation in female ESCs and female EGCs occurs evenly across the genome.

Methylation Patterns Are Driven by the Ratio of X Chromosomes to Autosomes

In light of our finding that sex correlates with DNA methylation patterns in both ESCs and EGCs, we next investigated whether the number of X chromosomes influences methylation levels using ESC-somatic and EGC-somatic hybrids (Figure 2A). Briefly, neomycin-resistant ESC and EGC lines of both sexes were fused to puromycin-resistant male or female mouse embryonic fibroblasts (MEFs) carrying an EGFP reporter in the endogenous *Pou5f1* locus (termed *Oct4-GFP*) using polyethylene glycol (PEG), followed by dual selection for G418 and puromycin (Figure 2A). We confirmed that hybrid clones reactivated the somatically silenced *Oct4-GFP* reporter and carried a predominantly tetraploid genome before measuring DNA methylation patterns by RRBS analysis (Figures 2B and 2C; Figures S3A and S3B).

Several important conclusions can be drawn from this analysis. First, overall methylation levels of male and female (4n) hybrids resembled those of the parental male and female (2n) pluripotent stem cell line, even though the (2n) somatic fusion partners of either sex (i.e., MEFs) were normally methylated (Figure 2D; Figures S2A and S3C). This result indicates that the female somatic genome in XXXX hybrids undergoes massive demethylation toward a female ESC- or EGC-like state while the male somatic genome remains comparatively methylated in XXYY hybrids (Figure 2D; Figure S3C). Considering that cell fusion between MEFs and ESCs or EGCs leads to the reactivation of the somatically silenced X chromosome (Tada et al., 2001), this finding implies that the ratio of X^A chromosomes to autosomes, rather than the absolute number of X chromosomes inside a pluripotent cell, dictates DNA methylation levels (Figure 2E). In support of this notion, we found that a haploid female (X) ESC line (Elling et al., 2011) was similarly hypomethylated as a diploid female (XX) or tetraploid female (XXXX) ESC line (Figures 2D and 2E). Pluripotency loci such as *Oct4* were equally demethylated in male and female hybrids, thus excluding the possibility that the observed sex-specific methylation differences were a consequence of incomplete reprogramming of the somatic genome or cellular differentiation (Figure S3A). We also confirmed the presence of either two or four X chromosomes in most male or female hybrids using FISH, although we observed some variability (Figure S3B). We believe that slight distortions to the X chromosome-to-autosome ratio resulting from this variability may explain the reduced global methylation levels in male hybrids compared to male diploid ESCs and EGCs (Figure 2D).

Second, global methylation levels of ESC hybrids were comparable to those of EGC hybrids of the same sex (Figure 2D). Examination of methylation patterns at promoter regions, LTRs, LINEs, and SINEs in ESC and EGC hybrids corroborated this conclusion (Figure S3C). Thus, sex rather than cell type determines global methylation levels in both ESC-somatic and EGC-somatic hybrids.

Third, imprinted gene methylation showed cell type and sex dependent differences (Figures 2F and 2G; Figure S3D). For example, male ESC hybrids showed methylation patterns similar to those of male parental MEFs or ESCs, whereas female ESC hybrids exhibited a marked reduction of methylation levels across most imprinted loci, consistent with a sex-specific effect (Figures 2F and 2G). In addition, we noticed a pronounced demethylation of imprinted genes in male EGC hybrids that was absent in male ESC hybrids, implying erasure of somatic imprints by an EGC-specific, sex-independent demethylation mechanism (Figures 2F and 2G) (Piccolo et al., 2013; Tada et al., 1997). Imprinted methylation was also reduced in female EGC hybrids compared to female ESC hybrids, although this difference was less striking than in male counterparts. In agreement with these results, unsupervised hierarchical clustering based on all imprinted genes separated male ESC hybrids (normally methylated) from female ESC hybrids and EGC hybrids of either sex (hypomethylated) (Figure 2G), phenocopying imprinting patterns of the parental pluripotent cell lines (Figure 1F). Altogether, these results show that global methylation patterns in ESC-somatic and EGC-somatic hybrids are dictated by the ratio of X^A chromosomes to autosomes, regardless of the origin of the pluripotent fusion partner, whereas imprinted gene methylation is influenced by both sex and cell type.

Male and Female Blastocysts Are Similarly Hypomethylated

The observation that sex correlates with methylation patterns in pluripotent cell lines regardless of cell type raises the important question of whether this reflects methylation differences in the ICM from which ESCs are derived. To prospectively identify male and female blastocysts, we crossed male mice carrying an X-linked GFP transgene (X^{GFP}Y) (Hadjantonakis et al., 2001) to wild-type female (XX) mice (Figure 3A). Isolated zygotes were flushed from the oviducts and cultured for 4 days in potassium-supplemented simplex optimized media (KSOM) until they formed expanded blastocysts with a discernible ICM. Approximately half of the blastocysts were GFP positive and female (X^{GFP}X), while the other half of the embryos were GFP negative and male (XY), as expected (Figure 3B). Significantly more GFP-negative blastocysts had already hatched by day 4 compared to GFP-positive blastocysts (Figures 3B and 3C), which is consistent with a slight acceleration of development in male relative to female preimplantation embryos (Burgoyne, 1993). We then dissected the ICM of each blastocyst by immunosurgery and subjected pools of male (n = 20) and female (n = 29) ICMs to RRBS analysis.

In contrast to cultured ESC lines, both male and female ICMs were equally hypomethylated when considering 1 kb tiles across the genome, reaching levels that were again similar to late-passage male *Dnmt3a/b* DKO ESCs (Figures 3D and 3E). We detected a small subset of loci with differential methylation

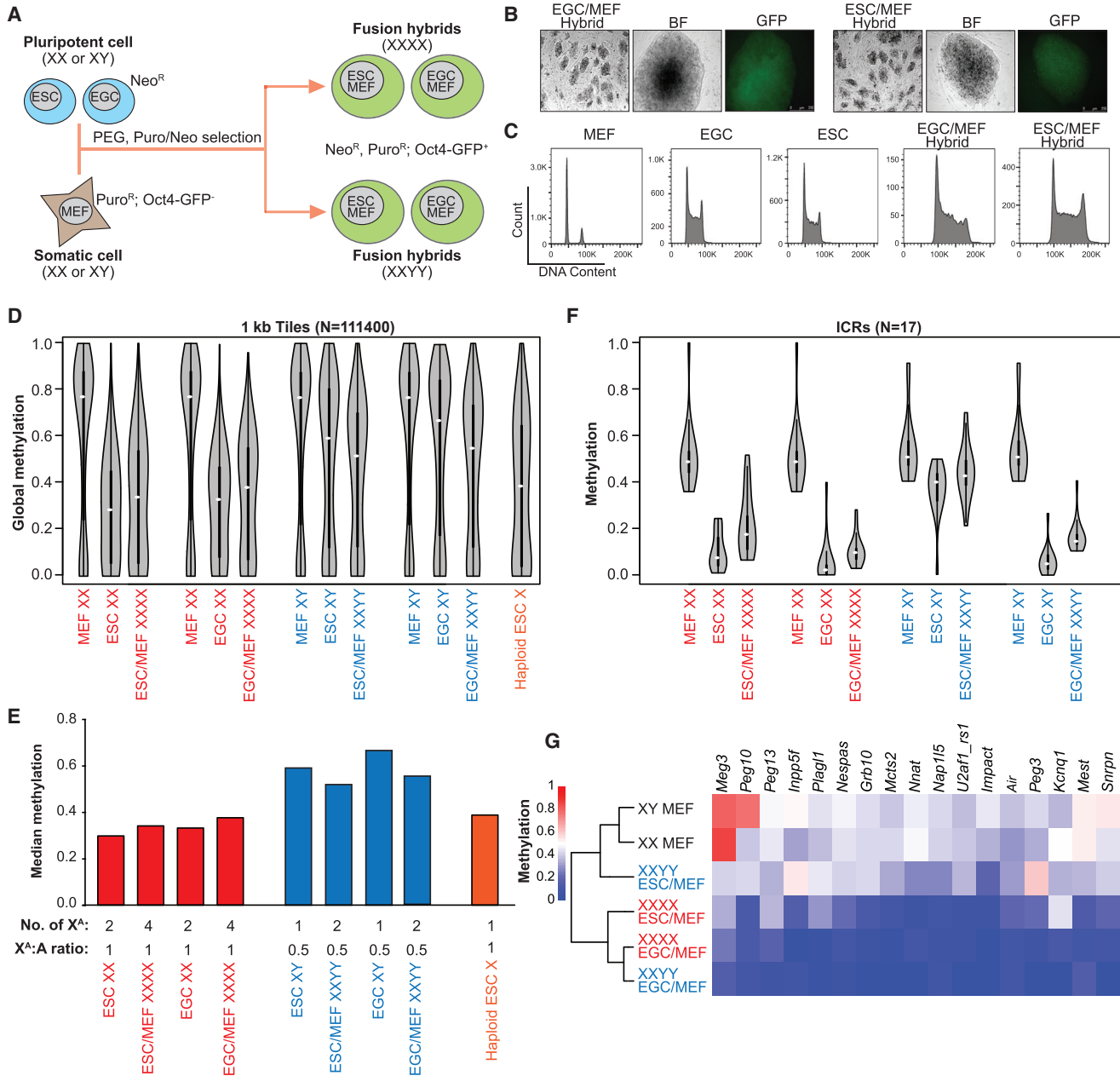


Figure 2. Ratio of X Chromosomes to Autosomes Correlates with Global Methylation Levels in Pluripotent Cell Lines

- (A) Schematic of the generation of ESC-somatic and EGC-somatic hybrids.
- (B) Representative ESC/MEF hybrids and EGC/MEF hybrids show activation of somatically silenced Oct4-EGFP reporter.
- (C) Representative EGC/MEF and ESC/MEF hybrids show tetraploid DNA content compared to parental fusion partners using propidium iodide (PI) staining.
- (D) Global methylation levels of 4n ESC-somatic and EGC-somatic hybrids and their respective 2n fusion partners as determined by RRBS analysis. White boxes indicate median methylation levels. One representative line for each cell type is shown. A haploid ESC (X) line was included as a control in (D) and (E).
- (E) Median global methylation levels of 4n hybrids and their respective 2n fusion partners from (D) are shown (top). The number of presumed active X (X^A) chromosomes for each line and the ratio of X^A chromosomes to autosomes (A) are shown (bottom).
- (F) Methylation levels of all captured imprinted loci from ESC-somatic and EGC-somatic hybrids and their fusion partners from (D) as measured by RRBS analysis. White boxes indicate median methylation levels.
- (G) Dendrogram and heatmap representation of imprinted methylation in ESC-somatic and EGC-somatic hybrids and their somatic fusion partners. Average methylation levels across ICRs of two XXYY ESC/MEF hybrids, two XXYY EGC/MEF hybrids, three XXXX ESC/MEF hybrids, three XXXX EGC/MEF hybrids, one XY MEF, and one XX MEF line are shown. Blue, XXYY hybrid; red, XXXX hybrid; black, XX and XY MEF.

See also Figure S3.

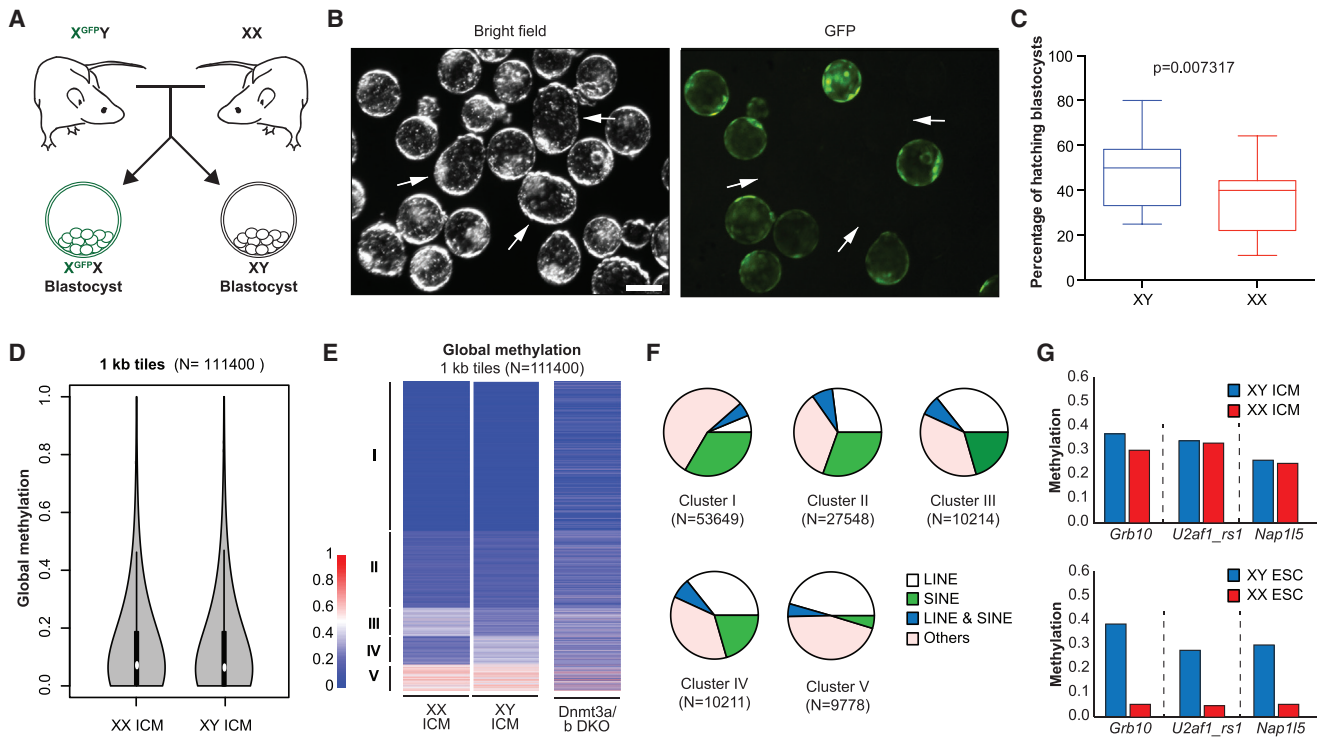


Figure 3. Male and Female ICMs Are Similarly Hypomethylated

(A) Schematic of the generation of $X^{GFP}X$ and XY blastocysts.

(B) Representative bright-field images of $X^{GFP}X$ and XY blastocysts (left) and GFP-positive $X^{GFP}X$ blastocysts (right) are shown. White arrows indicate hatching XY blastocysts.

(C) The percentage of hatching $X^{GFP}X$ and XY blastocysts from the same litter is plotted. 123 $X^{GFP}X$ and 104 XY blastocysts from 11 independent litters were scored. Data are judged to be statistically significant when $p < 0.05$ by two-tailed Student's t test. Error bars show the minimum and maximum values.

(D) Global methylation analysis of pooled XX ($n = 29$) and XY ($n = 20$) ICMs by RRBS using violin plot representation. White boxes indicate median methylation levels.

(E) Comparison of genome-wide DNA methylation patterns by RRBS in XX and XY ICMs. Global methylation patterns are classified into five clusters. The *Dnmt3a/b* DKO cell line was included as a control.

(F) Compositions of each cluster from (E) are shown as pie charts.

(G) Average methylation levels across imprinting control regions (ICRs) for indicated loci from ICM cells (top; 20 XY and 29 XX ICMs) and ESC cells (bottom; three XY and three XX lines).

See also Figure S4.

patterns between male and female ICMs (Figure 3E, clusters III and IV). Closer inspection revealed that more than two-thirds of these loci are associated with repetitive elements, including LINEs and SINEs (Figure 3F). Because repetitive elements undergo dynamic methylation changes during preimplantation development (Smith et al., 2014), we surmise that the apparent sex-specific methylation differences are due to the slight developmental asynchrony between male and female blastocysts (Burgoyne, 1993). Critically, male and female ICMs maintained methylation at ICRs that were eroded in cultured female ESC lines (Figure 3G; Figure S4). Altogether, these results show that male and female ICMs are equally hypomethylated and retain ICR methylation, pointing to profound sex- and culture-dependent methylation differences between pluripotent cells *in vivo* and those *ex vivo*.

Post-transcriptional Regulation of Epigenetic and Pluripotency Factors in Female ESCs

To elucidate the mechanisms that may be responsible for global DNA hypomethylation in female stem cells, we compared tran-

scriptional profiles of isogenic ESCs and EGCs from both sexes by RNA sequencing (RNA-seq) analysis. Unsupervised hierarchical clustering showed that female stem cells are grouped separately from male stem cells, which is consistent with our methylation data (Figure 4A). We determined mRNA levels of known regulators of DNA methylation in our dataset, assuming that they would be differentially regulated in male and female stem cells. With the exception of *Dnmt3l* and *Tet3*, expression levels of *Dnmt1*, *Uhrf1*, *Dnmt3a*, *Dnmt3b*, *Tet1*, and *Tet2* were not significantly different between male and female cell lines (Figure 4B; Figure S5A). However, we noticed striking differences at the protein level for these enzymes, with female cell lines showing substantially lower amounts of DNMT1, DNMT3A, and DNMT3B and increased amounts of TET2 relative to male cell lines (Figures 4C and 4D; Figures S5B–S5E).

To determine the scale of post-transcriptional gene expression differences between male and female ESCs, we performed proteomics analysis. We found that of roughly 8,300 proteins detected by tandem mass spectrometry, ~550 (7%) were differentially expressed between male ($n = 2$) and female ($n = 2$) ESCs

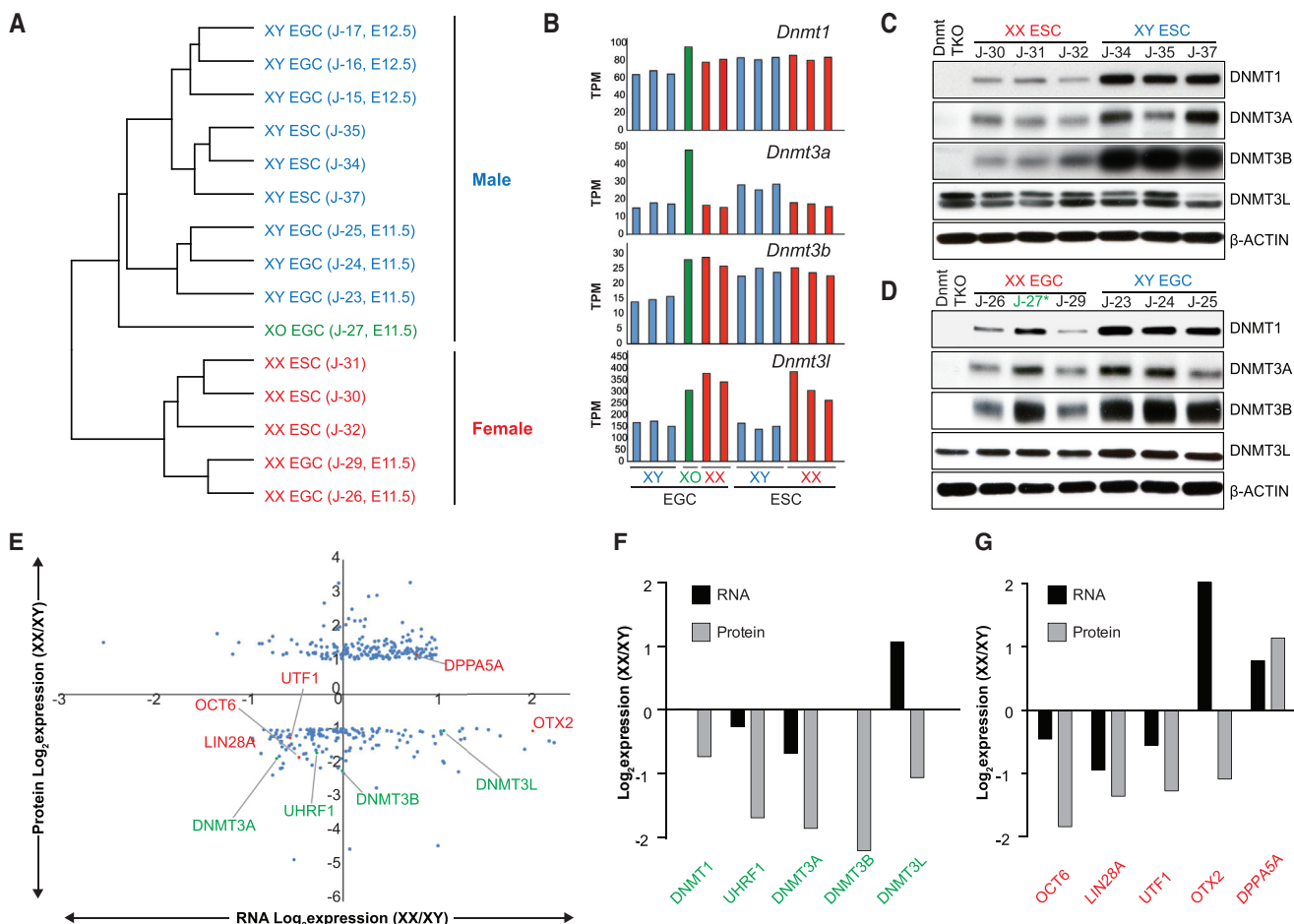


Figure 4. Post-transcriptional Regulation of Epigenetic and Pluripotency Factors in Female ESCs

(A) Unsupervised hierarchical clustering of RNA-seq data obtained from isogenic ESC and EGC lines.

(B) mRNA levels for *Dnmt1*, *Dnmt3a*, *Dnmt3b*, and *Dnmt3l* in isogenic ESC and EGC lines.

(C and D) Western blot analyses for DNMT1, DNMT3A, DNMT3B, and DNMT3L in isogenic XX and XY ESC (C) and EGC (D) lines. See Figures S5B and S5C for quantification. Blue represents XY cells, red represents XX cells, and green (*) represents the XO cell line.

(E) Correlation between RNA-seq data (three XX and three XY ESC lines) and proteomics data (two replicates per ESC line). 193 proteins were found to be upregulated in female ESCs compared to male ESCs even though corresponding RNAs did not change ($n = 189$) or were downregulated ($n = 4$). By contrast, 161 proteins were found to be downregulated in female ESCs compared to male ESCs even though corresponding RNAs did not change ($n = 143$) or were upregulated ($n = 18$). Differentially expressed proteins between male and female ESCs (>2-fold) were plotted along the y axis; corresponding differentially expressed RNAs were plotted along the x axis. Expression levels of DNA methyltransferases and cofactors (green), as well as naive and primed pluripotency markers (red), are highlighted.

(F) Differential expression of DNA methyltransferases and cofactors from (E) (green) is shown at the RNA (black) and protein (gray) levels.

(G) Differential expression of naive or primed pluripotency markers from (E) (red) is shown at the RNA (black) and protein (gray) levels.

See also Figure S5 and Tables S1, S2, S3, S4, and S7.

(Table S1). A comparison of our RNA-seq and proteomics data further showed that 143 proteins were downregulated and 189 proteins were upregulated in female ESCs relative to male ESCs even though associated RNA levels remained unchanged (Figure 4E; Tables S2 and S3). This analysis confirmed reduced protein levels for DNMT1, DNMT3A, and DNMT3B despite minor or no changes of RNA levels (Figures 4E and 4F). In addition, we identified UHRF1 among the downregulated proteins with constant RNA levels in female ESCs. We failed to detect differential RNA or protein expression for other factors that have previously been implicated in genomic methylation (Figure S5F), including KDM2B (Boulard et al., 2015), CXCC1 (Carlone et al., 2005),

and HELLS (Dennis et al., 2001). Similar to the aforementioned post-transcriptional regulation of epigenetic regulators, we noticed reduced protein levels for several factors associated with primed pluripotency, such as OTX2, LIN28A, OCT6, and UTF1, and higher protein levels for DPPA5A, a factor associated with naive pluripotency in female ESCs (Figures 4E and 4G). Combined with the elevated expression of TET2, NANOG, and SATB2 at the protein level (Figures S5D, S5E, and S5G), this observation supports the view that female ESCs may be molecularly closer to a naive state than male ESCs. Altogether, these results show that female ESCs are distinguished from male ESCs by the post-transcriptional regulation of hundreds of

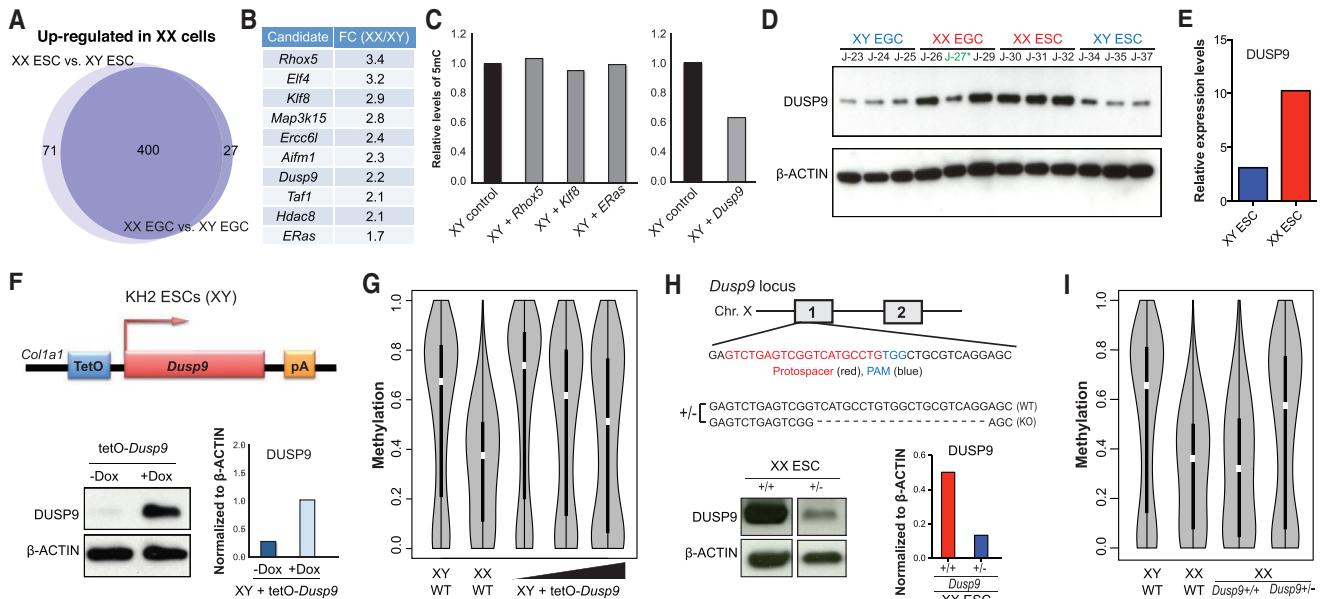


Figure 5. X-Linked *Dusp9* Gene Regulates Global DNA Hypomethylation in Female Stem Cells

- (A) Upregulated X-linked genes in XX EGC ($n = 2$) and ESC ($n = 3$) lines relative to XY counterparts (three EGC and three ESC lines).
- (B) List of candidate X-linked genes and their expression levels in XX stem cells compared to XY stem cells. FC, fold change.
- (C) Four candidate genes (*RhoX5*, *Klf8*, and *ERas*; left) and (*Dusp9*; right) from (B) were individually overexpressed in a XY ESC line, and global DNA methylation levels were subsequently examined by 5mC dot blot analysis. Global DNA methylation levels of each line were normalized to parental, wild-type ESCs.
- (D) Western blot analysis for DUSP9 in isogenic XX and XY ESCs and EGCs. See Figure S6A for quantification. Blue represents XY cells, red represents XX cells, and green (*) represents the XO cell line.
- (E) Mass-spectrometric quantification of DUSP9 protein levels in XY (blue; two replicates) and XX (red; two replicates) ESC lines.
- (F) Schematic (top) of doxycycline-inducible *Dusp9* allele introduced into KH2 (male) ESCs; these cells also carry a *ROSA26-M2rtTA* allele. Western blot analysis (bottom) for DUSP9 in *Dusp9*-overexpressing KH2 cells treated with or without doxycycline (left), plus quantification (right).
- (G) Global methylation analysis of *Dusp9*-overexpressing KH2 cells (with or without the additional *Dusp9* lentiviral overexpression construct) by RRBS using violin plot representation. White boxes indicate median methylation levels. XX and XY ESCs were included as controls.
- (H) Schematic (top) of heterozygous deletion of *Dusp9* alleles in a female 129xCast hybrid ESC line using CRISPR/Cas9 technology. Western blot analysis (bottom) for DUSP9 in *Dusp9*^{+/+} and *Dusp9*⁺⁻ ESC lines (left), plus quantification (right).
- (I) Global methylation analysis of the *Dusp9*^{+/+} and *Dusp9*⁺⁻ ESC lines by RRBS using violin plot representation. White boxes indicate median methylation levels. Wild-type 129xB6 XX and XY ESC lines were included as controls.

See also Figure S6 and Table S5.

genes, including transcription factors and epigenetic regulators associated with naive and primed pluripotency.

DUSP9 Is a Dose-Dependent Modulator of Female Hypomethylation

We next searched for candidate modulators of female hypomethylation that are more abundantly expressed in female compared to male ESCs and X-linked based on the observation that XO stem cells regain DNA methylation (Figure 1D; Figures S2C–S2E) (Zvetkova et al., 2005). Using our RNA-seq data, we identified 400 X-linked genes that were commonly upregulated in female EGCs and ESCs compared to male EGCs and ESCs, respectively (Figure 5A; Tables S4 and S5). We further narrowed down these candidates by searching for transcription factors and signaling modulators previously implicated in ESC self-renewal, including ERAS (Takahashi et al., 2003), DUSP9 (Li et al., 2012), and RHOX5 (also termed PEM) (Fan et al., 1999). We also selected KLF8, because other KLF family members were reported to support ESC self-renewal (Figure 5B) (Jiang et al., 2008). We then cloned cDNAs encoding for the respective factors into lentiviral vectors carrying a constitutive GFP or

Tomato reporter, infected male ESCs, sorted GFP- or Tomato-positive cells, and harvested cultures before conducting 5mC dot blot analysis. Although overexpression of ERAS, RHOX5, and KLF8 had no measurable effect on methylation levels, we detected a reduction of 5mC levels in DUSP9-overexpressing ESCs (Figure 5C). We confirmed elevated DUSP9 protein levels in female compared to male ESCs and EGCs using western blot analysis and our proteomics data of ESCs (Figures 5D and 5E; Figure S6A). DUSP9 is a dual-specificity phosphatase that inhibits mitogen-activated protein kinases (MAPKs) with preference for ERK, followed by p38 and JNK (Caunt and Keyse, 2013). This may explain the previous observation that MAPK signaling is reduced in female ESCs (Schulz et al., 2014). Moreover, the genes encoding for DUSP9's known substrates (i.e., *Erk1/2*, *p38 α* , and *Jnk1/2/3*) are present on autosomes, which fits with our finding that the X^A chromosome-to-autosome ratio is critical for DNA methylation levels in pluripotent cells.

To study the effects of DUSP9 expression on DNA methylation in a more defined and controllable system, we introduced a doxycycline-inducible single-copy transgene of *Dusp9* into the *Col1a1* locus of male KH2 ESCs (Figure 5F) (Beard et al., 2006).

Exposure of this engineered cell line to doxycycline led to DUSP9 upregulation and a concomitant reduction of global methylation levels by ~15% (Figure 5G; Figure S6B). Infection of this transgenic cell line with a dox-inducible virus expressing additional DUSP9 protein reduced 5mC levels by ~30%, indicating that DUSP9 modulates global methylation levels in a dose-dependent manner over multiple passages. We found that a female ESC line analyzed at the same time showed a similar reduction of methylation levels (~40%) relative to an isogenic male ESC control (Figure 5G).

Considering that overexpression of DUSP9 is sufficient to reduce methylation levels in male ESCs, we next tested whether *Dusp9* may also be required to maintain hypomethylation in female ESCs. To this end, we deleted one *Dusp9* allele in a female 129xCastaneous (129xCast) hybrid ESC line using CRISPR/Cas9 technology before conducting RRBS; we chose 129xCast ESCs because they were previously shown to maintain both X chromosomes upon extended culture (Figure 5H) (Lee and Lu, 1999). Even though the unmodified 129xCast ESC line was hypomethylated to a similar extent as our female 129xB6 hybrid ESC lines, *Dusp9^{+/−}* derivatives approached male ESC-like methylation levels despite the presence of two X chromosomes (Figure 5I; Figure S6C). Elevated methylation levels in *Dusp9^{+/−}* ESC lines were only detected after several rounds of passaging, implying a passive, replication-dependent process. Critically, we excluded that these increased methylation levels were due to differentiated cells by sorting cells for the ESC-specific marker SSEA1 before RRBS analysis and by confirming demethylation of endogenous pluripotency loci, including *Pou5f1*, *Zfp42* (*Rex1*), and *Dppa4*, in the *Dusp9^{+/−}* sample (Figure S6D). Unsupervised hierarchical clustering of all RRBS samples based on promoter methylation further showed that male ESCs overexpressing DUSP9 were more similar to wild-type female ESCs, whereas female ESCs lacking one *Dusp9* allele were more similar to wild-type male ESCs (Figures S6E and S6F). We conclude that DUSP9 is a dose-dependent modulator of global methylation levels in pluripotent stem cell lines, whereby DUSP9 overexpression is sufficient to induce partial hypomethylation in male ESCs while heterozygous *Dusp9* deletion increases methylation levels in female ESCs.

DUSP9 Overexpression Establishes a Female-like Proteome and Signaling State in Male ESCs

Female ESCs reportedly express lower levels of MAPK and GSK3 targets and higher levels of AKT targets compared to male ESCs, which is reminiscent of naive culture conditions and may underlie the observed female-specific hypomethylation (Schulz et al., 2014). To determine whether DUSP9 overexpression in male ESCs is sufficient to recapitulate this female-like signaling state, we performed western blot analysis for the activated forms of the MAPKs MEK1/2 (phospho-MEK1/2 [p-MEK1/2]) and their downstream kinases ERK1/2 (phospho-ERK1/2 [p-ERK1/2]). Like female ESCs, p-MEK1/2 and p-ERK1/2 levels were increased rather than decreased in DUSP9-overexpressing male ESCs, consistent with compensatory feedback mechanisms due to downregulation of a downstream component or components of the MAPK pathway (Figure 6A; Figure S7A) (Schulz et al., 2014). Proteomics analysis showed that expression of several downstream targets of the

MAPK and GSK3 pathways were reduced while targets of the AKT pathway were increased in DUSP9-overexpressing ESCs, mirroring the signaling state of female ESCs (Figure 6B). These results also suggest that DUSP9 overexpression inhibits the MAPK pathway downstream of, or parallel to, MEK/ERK by a yet-to-be-identified target (Figure 6C).

Global analysis of proteomics data revealed that ~700 proteins were up- or downregulated in DUSP9-overexpressing ESCs compared to uninduced controls (Figure 6D; Tables S6 and S7). About a third of these peptides (222) overlapped with proteins whose levels were different between male and female ESCs, suggesting that DUSP9 overexpression partially instates a female-like proteome in male ESCs. For example, we noticed reduced levels of the primed pluripotency markers DNMT3B, ZIC2, and MYCN but increased levels of the naive pluripotency markers TFCP2L1, ROR2, and PRDM14 in both DUSP9-overexpressing male ESCs and female ESCs relative to untreated male ESCs (Figure 6E). Moreover, DUSP9 overexpression led to an increase of DUSP7 levels yet a decrease of DUSP27 levels akin to female ESCs, suggesting complex cross-regulation among DUSP family members. Western blot analysis confirmed downregulation of DNMT3B and showed that DNMT3A and DNMT3L levels were also reduced upon DUSP9 overexpression, consistent with our observations in female ESCs (Figure 6F; Figure S7B). However, DNMT1 levels remained unchanged and UHRF1 levels only slightly decreased after DUSP9 overexpression, possibly explaining the less pronounced demethylation phenotype compared to female ESCs (Figure 6F; Figure S7C). Collectively, these findings show that DUSP9 overexpression partially phenocopies female-specific modulation of signaling pathways, epigenetic regulators, and pluripotency-associated transcription factors, providing a mechanistic basis for the observed hypomethylation.

DISCUSSION

Here, we show that EGC and ESC lines are highly similar with regards to global transcriptional and DNA methylation patterns when comparing cell lines within the same sex (Figure 7A). Our results may explain previous observations, which suggested that late-stage EGCs, in comparison with ESCs, are globally less methylated, express higher levels of NANOG, and induce more extensive demethylation of repetitive elements in fusion hybrids (Hatano et al., 2005; Tada et al., 1997, 2001). Re-examination of these prior studies reveals that methylation, protein, and fusion assays were performed with female EGCs and female somatic cells, whereas ESC controls were of male origin. Earlier studies had detected reduced methylation of repetitive elements or imprinted loci when comparing female to male EGC lines derived from either E8.5 or E11.5–E12.5 genital ridges using Southern blot analysis (Durcova-Hills et al., 2004; Shovlin et al., 2008; Tada et al., 1998). However, a subsequent, comprehensive comparison of E8.5 EGCs and genetically matched ESCs failed to find sex-specific methylation or expression differences using bisulfite sequencing (Leitch et al., 2013). We believe that variability due to culture methods and methylation assays or the use of early-stage (E8.5) versus late-stage (E12.5) EGCs may account for the observed differences. It is further possible that some previously studied female cell lines were afflicted by

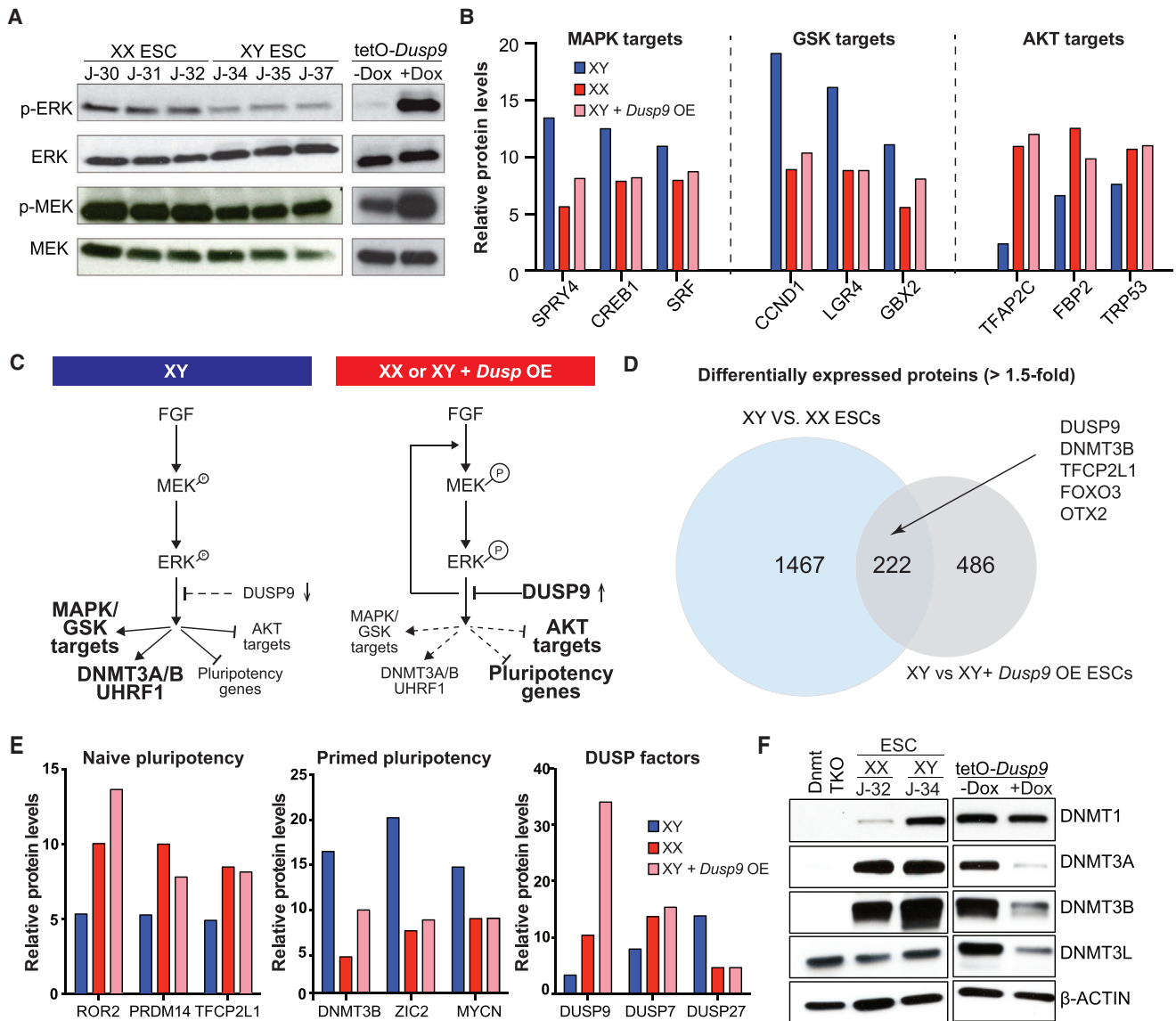


Figure 6. DUSP9 Overexpression Establishes a Female-like Proteome and Signaling State in Male ESCs

- (A) Western blot analyses for p-ERK, ERK, p-MEK, and MEK in isogenic XX and XY ESCs (left) and in *Dusp9*-overexpressing KH2 cells (right). See Figure S7A for quantification.
- (B) Expression of targets of ERK, GSK, and AKT pathways in XY (blue) and XX (red) ESCs, as well as *Dusp9*-overexpressing KH2 cells treated with doxycycline (pink), using proteomics data (two replicates per line).
- (C) Model to explain dose-dependent regulation of MAPK/GSK/AKT pathways, pluripotency, and epigenetic factors by DUSP9.
- (D) Venn diagram of differentially expressed proteins (>1.5-fold) between male and female ESCs (blue) and between wild-type male ESCs and *Dusp9*-overexpressing male ESCs (gray). Examples of overlapping proteins are indicated by an arrow.
- (E) Expression of proteins associated with naive and primed pluripotency, along with DUSP factors, in XY (blue) and XX (red) ESCs, as well as *Dusp9*-overexpressing KH2 ESCs treated with doxycycline (pink), using proteomics data (two replicates per line).
- (F) Western blot analysis for DNMT1, DNMT3A, DNMT3B, and DNMT3L levels in *Dusp9*-overexpressing KH2 cells treated with or without doxycycline. A *Dnmt1/3a/b* triple-knockout (TKO) male ESC line and wild-type XX and XY ESC lines were included as controls. See Figure S7B for quantification.
- See also Figure S7 and Tables S1 and S6.

X chromosome loss, which would mask methylation differences. Our use of 129xB6 hybrid cell lines may be another reason for differences observed between this study and previous studies that used inbred EGC and ESC lines. Although we were unable to detect methylation differences between ESCs and EGCs of the same sex when analyzing CpG islands and shores, LINEs,

SINEs, and LTRs, our data support the previous finding that imprinted genes are more susceptible to demethylation in male EGC hybrids compared to male ESC hybrids (Piccolo et al., 2013; Tada et al., 1997).

Our data suggest that the ratio of X^A chromosomes to autosomes dictates methylation levels in mouse pluripotent stem

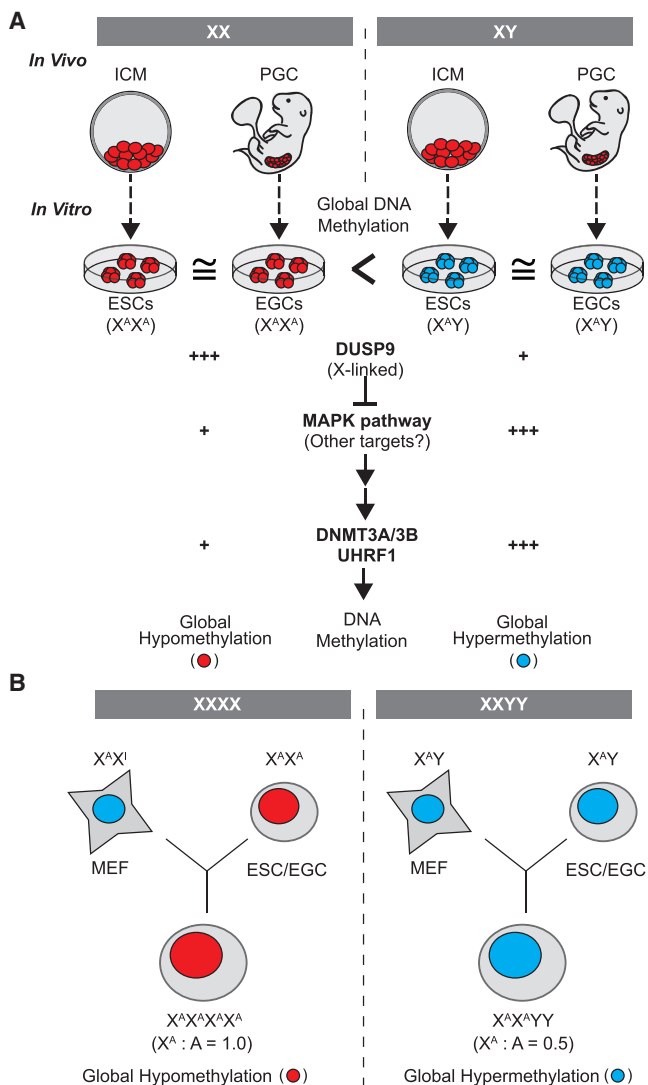


Figure 7. Effect of Sex Chromosomes and Associated Signaling Pathways on DNA Methylation in Pluripotent Cells

(A) Both ICM cells and PGCs are globally hypomethylated during development, regardless of sex. However, ESCs and EGCs, derived from explanted ICM cells and PGCs, exhibit distinct DNA methylation status according to their sex. Female ESCs and EGCs maintain global hypomethylation, which is partly because of elevated expression of the X-linked *Dusp9* gene. Upregulation of *Dusp9* attenuates MAPK signaling and, directly or indirectly, leads to downregulation of DNMT3A/B and UHRF1.

(B) Global DNA methylation levels in fusion hybrids between MEFs and either ESCs or EGCs are dictated by the ratio of active X (X^A) chromosomes to autosomes (As) rather than the absolute number of X^A chromosomes.

Red, global DNA hypomethylation; blue, global DNA hypermethylation. X^I , inactive X chromosome.

cells, and we have ascribed this phenotype in part to the upregulation of *Dusp9* in female ESCs (Figure 7B). We show that heterozygous deletion of the X-linked MAPK phosphatase *Dusp9* in female ESCs leads to increased global methylation over time while its overexpression in male ESCs induces partial hypomethylation, providing a molecular link between X chromosome dosage, MAPK signaling, and genomic methylation (Figure 7A).

Our inability to fully recapitulate female-specific hypomethylation upon *Dusp9* overexpression in male ESCs could be due to (1) poor activity of overexpressed *Dusp9*, (2) insufficient time to (passively) demethylate the genome, or (3) the involvement of other X-linked genes that act in parallel to *Dusp9*. We recognize that the mechanisms underlying female-specific hypomethylation may be similar, but not identical, to that of 2i-induced hypomethylation. While 2i-induced hypomethylation reportedly involves transcriptional repression of *Dnmt3a/b* and activation of *Tet1/2* by the transcription factors PRDM14 and NANOG (Ficz et al., 2013; Hackett et al., 2013; Okashita et al., 2014; Yamaji et al., 2013), our results suggest that female-specific hypomethylation involves a mechanism that operates predominantly through post-transcriptional destabilization of DNMT1/3A/B and their cofactors UHRF1 and DNMT3L. The recent observation that reduced protein levels of UHRF1 are also critical for 2i-induced hypomethylation (von Meyenn et al., 2016) supports a mechanistic overlap between naive culture conditions and female-specific hypomethylation. Our finding that *Dusp9* overexpression leads to the downregulation of MAPK and GSK3 targets and proteins associated with primed pluripotency but upregulation of factors associated with naive pluripotency further underscores the molecular similarity to 2i culture, although these results do not show that female ESCs are in a bona fide naive pluripotent state. While 2i directly inhibits MEK1/2 and GSK3, *Dusp9* seems to suppress these pathways downstream of ERK1/2 by target proteins that remain to be identified.

The dramatic differences in global methylation between male and female pluripotent stem cell lines do not extend to the ICMs of male and female blastocysts, which showed equally low 5mC levels and stable retention of ICR methylation (Figure 7A). This unexpected finding underscores the profound effects that explantation and continuous propagation of pluripotent cells ex vivo can have on the epigenome of ESCs. Despite these differences between ICM cells and derivative ESCs, our observations in cultured stem cells may be relevant for understanding epigenetic processes in vivo. For example, while both male and female primordial germ cells (PGCs) are globally hypomethylated, female PGCs, like female pluripotent cell lines, carry two active X chromosomes and exhibit a more pronounced reduction of global methylation levels relative to male PGCs (Popp et al., 2010). Similar to our cultured female ESCs, human PGCs express reduced levels of UHRF1 and DNMT3A at the protein level, but not the RNA level, and this has been associated with global demethylation (Oliveros-Etter et al., 2015). Considering this association between female cells with two X^A chromosomes and hypomethylation, it should be interesting to explore whether relaxation of X chromosome inactivation in somatic cells affects DNA methylation patterns (Yang et al., 2016). Moreover, it would be informative to assess whether *Dusp9*-deficient embryos, which succumb to placental defects early in development (Christie et al., 2005), exhibit aberrant methylation patterns within the embryonic or extra-embryonic compartments.

In summary, our data provide new molecular insights into the role of sex chromosomes and associated signaling pathways on the epigenetic state of distinct pluripotent stem cells. Our data further clarify some of the discrepancies surrounding methylation differences between ESCs and (late-stage) EGCs and emphasize the importance of controlling for sex, genetic

background, and culture conditions when assessing the epigenome and transcriptome of pluripotent stem cell lines.

STAR METHODS

Detailed methods are provided in the online version of this paper and include the following:

- KEY RESOURCES TABLE
- CONTACT FOR REAGENT AND RESOURCE SHARING
- EXPERIMENTAL MODEL AND SUBJECT DETAILS
 - Animal care and use
 - Mouse ESC generation
 - Mouse EGC generation
- METHODS DETAILS
 - Cell fusion
 - Teratoma assay
 - Blastocyst injection
 - Immunosurgery
 - AP Staining and immunostaining
 - Bisulfite Sequencing
 - Southern blot analysis for global DNA methylation
 - Dot blot assay
 - Reduced representation bisulfite sequencing (RRBS)
 - RNA-sequencing
 - RNA-seq data analysis
 - Western blot analysis
 - Gene targeting of ESCs
 - Viral production
 - Generation of *Dusp9^{+/−}* *M. musculus* × *M. castaneous* ESCs
 - X chromosome FISH
 - Proteomic sample preparation
 - Mass spectrometry analysis
 - Mass spectrometry data analysis
- QUANTIFICATION AND STATISTICAL ANALYSIS
- DATA AND SOFTWARE AVAILABILITY
 - Software
 - Data resources

SUPPLEMENTAL INFORMATION

Supplemental Information includes seven figures and seven tables and can be found with this article online at <http://dx.doi.org/10.1016/j.stem.2017.03.002>.

AUTHOR CONTRIBUTIONS

Conceptualization, J.C., K.C., A.M., and K.H.; Methodology, J.C.; Investigation, J.C., A.J.H., J.W., J.B., R.M.W., and J.-P.E.; Formal Analysis, K.C., C.M.R., S.L., and A.S.; Resources, H.G., P.B., and U.E.; Writing – Original Draft, J.C. and K.C.; Writing – Review & Editing, A.M. and K.H.; Visualization, J.C.; Supervision, R.M., R.S., P.J.P., S.P.G., A.M., and K.H.; Funding Acquisition, A.M. and K.H.

ACKNOWLEDGMENTS

We thank members of the Hochedlinger and Meissner labs for helpful comments and critical reading of the manuscript. We thank K. Folz-Donahue, M. Weglarz, L. Prickett, A. Galvin, M. Gesner, and A. Handley at the Massachusetts General Hospital/Harvard Stem Cell Institute flow cytometry core. We are grateful to A.L. Hawkins, S. Wang, A. Aggarwal, and C.C. Morton at Brigham and Woman's Hospital CytoGenomics Core Laboratory for FISH analysis.

We thank J. Lee for providing the EL16.7 female ESC line and X-linked GFP mice. We also thank L. Yan at EpigenDx for bisulfite methylation sequencing. A.J.H. was supported by an American Cancer Society, New England Division, Ellison Foundation Postdoctoral Fellowship (PF-15-130-01-DDC). J.B. was supported by the NIH (1F32HD078029-01A1). A.M. was supported by the NIH (P01GM099117), the New York Stem Cell Foundation, and the Center for Excellence in Genome Science from the NHGRI (1P50HG006193-01). A.M. is a New York Stem Cell Foundation Robertson Investigator. K.H. was supported by HHMI, the NIH (R01 HD058013), and the Gerald R. and Darlene Jordan Endowed Chair for Regenerative Medicine.

Received: September 9, 2016

Revised: December 12, 2016

Accepted: March 6, 2017

Published: March 30, 2017

REFERENCES

- Anders, S., McCarthy, D.J., Chen, Y., Okoniewski, M., Smyth, G.K., Huber, W., and Robinson, M.D. (2013). Count-based differential expression analysis of RNA sequencing data using R and Bioconductor. *Nat. Protoc.* 8, 1765–1786.
- Beard, C., Hochedlinger, K., Plath, K., Wutz, A., and Jaenisch, R. (2006). Efficient method to generate single-copy transgenic mice by site-specific integration in embryonic stem cells. *Genesis* 44, 23–28.
- Boulard, M., Edwards, J.R., and Bestor, T.H. (2015). FBXL10 protects Polycomb-bound genes from hypermethylation. *Nat. Genet.* 47, 479–485.
- Burgoyne, P.S. (1993). A Y-chromosomal effect on blastocyst cell number in mice. *Development* 117, 341–345.
- Carlone, D.L., Lee, J.-H., Young, S.R.L., Dobrota, E., Butler, J.S., Ruiz, J., and Skalnik, D.G. (2005). Reduced genomic cytosine methylation and defective cellular differentiation in embryonic stem cells lacking CpG binding protein. *Mol. Cell. Biol.* 25, 4881–4891.
- Caunt, C.J., and Keyse, S.M. (2013). Dual-specificity MAP kinase phosphatases (MKPs): shaping the outcome of MAP kinase signalling. *FEBS J.* 280, 489–504.
- Chen, A.E., and Melton, D.A. (2007). Derivation of human embryonic stem cells by immunosurgery. *J. Vis. Exp.* 10, 574.
- Christie, G.R., Williams, D.J., Macisaac, F., Dickinson, R.J., Rosewell, I., and Keyse, S.M. (2005). The dual-specificity protein phosphatase DUSP9/MKP-4 is essential for placental function but is not required for normal embryonic development. *Mol. Cell. Biol.* 25, 8323–8333.
- Dennis, K., Fan, T., Geiman, T., Yan, Q., and Muegge, K. (2001). Lsh, a member of the SNF2 family, is required for genome-wide methylation. *Genes Dev.* 15, 2940–2944.
- Durcova-Hills, G., Burgoyne, P., and McLaren, A. (2004). Analysis of sex differences in EGC imprinting. *Dev. Biol.* 268, 105–110.
- Eggan, K., Akutsu, H., Loring, J., Jackson-Grusby, L., Klemm, M., Rideout, W.M., 3rd, Yanagimachi, R., and Jaenisch, R. (2001). Hybrid vigor, fetal overgrowth, and viability of mice derived by nuclear cloning and tetraploid embryo complementation. *Proc. Natl. Acad. Sci. USA* 98, 6209–6214.
- Elias, J.E., and Gygi, S.P. (2007). Target-decoy search strategy for increased confidence in large-scale protein identifications by mass spectrometry. *Nat. Methods* 4, 207–214.
- Elling, U., Taubenschmid, J., Wirnsberger, G., O'Malley, R., Demers, S.-P., Vanhaelen, Q., Shukalyuk, A.I., Schmauss, G., Schramek, D., Schnuetgen, F., et al. (2011). Forward and reverse genetics through derivation of haploid mouse embryonic stem cells. *Cell Stem Cell* 9, 563–574.
- Eng, J.K., McCormack, A.L., and Yates, J.R. (1994). An approach to correlate tandem mass spectral data of peptides with amino acid sequences in a protein database. *J. Am. Soc. Mass Spectrom.* 5, 976–989.
- Erickson, B.K., Jedrychowski, M.P., McAlister, G.C., Everley, R.A., Kunz, R., and Gygi, S.P. (2015). Evaluating multiplexed quantitative phosphopeptide analysis on a hybrid quadrupole mass filter/linear ion trap/orbitrap mass spectrometer. *Anal. Chem.* 87, 1241–1249.

- Fan, Y., Melhem, M.F., and Chaillet, J.R. (1999). Forced expression of the homeobox-containing gene Pem blocks differentiation of embryonic stem cells. *Dev. Biol.* 210, 481–496.
- Ficz, G., Hore, T.A., Santos, F., Lee, H.J., Dean, W., Arand, J., Krueger, F., Oxley, D., Paul, Y.-L., Walter, J., et al. (2013). FGF signaling inhibition in ESCs drives rapid genome-wide demethylation to the epigenetic ground state of pluripotency. *Cell Stem Cell* 13, 351–359.
- Habibi, E., Brinkman, A.B., Arand, J., Kroeze, L.I., Kerstens, H.H.D., Matarese, F., Lepikhov, K., Gut, M., Brun-Heath, I., Hubner, N.C., et al. (2013). Whole-genome bisulfite sequencing of two distinct interconvertible DNA methylomes of mouse embryonic stem cells. *Cell Stem Cell* 13, 360–369.
- Hackett, J.A., Dietmann, S., Murakami, K., Down, T.A., Leitch, H.G., and Surani, M.A. (2013). Synergistic mechanisms of DNA demethylation during transition to ground-state pluripotency. *Stem Cell Reports* 1, 518–531.
- Hadjantonakis, A.K., Cox, L.L., Tam, P.P., and Nagy, A. (2001). An X-linked GFP transgene reveals unexpected paternal X-chromosome activity in trophoblastic giant cells of the mouse placenta. *Genesis* 29, 133–140.
- Hajkova, P., Jeffries, S.J., Lee, C., Miller, N., Jackson, S.P., and Surani, M.A. (2010). Genome-wide reprogramming in the mouse germ line entails the base excision repair pathway. *Science* 329, 78–82.
- Hatano, S.-Y., Tada, M., Kimura, H., Yamaguchi, S., Kono, T., Nakano, T., Suemori, H., Nakatsuji, N., and Tada, T. (2005). Pluripotential competence of cells associated with Nanog activity. *Mech. Dev.* 122, 67–79.
- Hutlin, E.L., Jedrychowski, M.P., Elias, J.E., Goswami, T., Rad, R., Beausoleil, S.A., Villén, J., Haas, W., Sowa, M.E., and Gygi, S.P. (2010). A tissue-specific atlas of mouse protein phosphorylation and expression. *Cell* 143, 1174–1189.
- Hwang, W.Y., Fu, Y., Reyon, D., Maeder, M.L., Tsai, S.Q., Sander, J.D., Peterson, R.T., Yeh, J.-R.J., and Joung, J.K. (2013). Efficient genome editing in zebrafish using a CRISPR-Cas system. *Nat. Biotechnol.* 31, 227–229.
- Isasa, M., Rose, C.M., Elsasser, S., Navarrete-Perea, J., Paulo, J.A., Finley, D.J., and Gygi, S.P. (2015). Multiplexed, proteome-wide protein expression profiling: yeast deubiquitylating enzyme knockout strains. *J. Proteome Res.* 14, 5306–5317.
- Jiang, J., Chan, Y.-S., Loh, Y.-H., Cai, J., Tong, G.-Q., Lim, C.-A., Robson, P., Zhong, S., and Ng, H.-H. (2008). A core Klf circuitry regulates self-renewal of embryonic stem cells. *Nat. Cell Biol.* 10, 353–360.
- Labosky, P.A., Barlow, D.P., and Hogan, B.L. (1994). Mouse embryonic germ (EG) cell lines: transmission through the germline and differences in the methylation imprint of insulin-like growth factor 2 receptor (*Igf2r*) gene compared with embryonic stem (ES) cell lines. *Development* 120, 3197–3204.
- Lee, J.T., and Lu, N. (1999). Targeted mutagenesis of *Tsix* leads to nonrandom X inactivation. *Cell* 99, 47–57.
- Leitch, H.G., Blair, K., Mansfield, W., Ayetey, H., Humphreys, P., Nichols, J., Surani, M.A., and Smith, A. (2010). Embryonic germ cells from mice and rats exhibit properties consistent with a generic pluripotent ground state. *Development* 137, 2279–2287.
- Leitch, H.G., McEwen, K.R., Turp, A., Encheva, V., Carroll, T., Grable, N., Mansfield, W., Nashun, B., Knezovich, J.G., Smith, A., et al. (2013). Naive pluripotency is associated with global DNA hypomethylation. *Nat. Struct. Mol. Biol.* 20, 311–316.
- Li, Z., Fei, T., Zhang, J., Zhu, G., Wang, L., Lu, D., Chi, X., Teng, Y., Hou, N., Yang, X., et al. (2012). BMP4 signaling acts via dual-specificity phosphatase 9 to control ERK activity in mouse embryonic stem cells. *Cell Stem Cell* 10, 171–182.
- Liao, J., Karnik, R., Gu, H., Ziller, M.J., Clement, K., Tsankov, A.M., Akopian, V., Gifford, C.A., Donaghey, J., Galonska, C., et al. (2015). Targeted disruption of DNMT1, DNMT3A and DNMT3B in human embryonic stem cells. *Nat. Genet.* 47, 469–478.
- Matsui, Y., Zsebo, K., and Hogan, B.L. (1992). Derivation of pluripotential embryonic stem cells from murine primordial germ cells in culture. *Cell* 70, 841–847.
- Meissner, A., Gnrke, A., Bell, G.W., Ramsahoye, B., Lander, E.S., and Jaenisch, R. (2005). Reduced representation bisulfite sequencing for comparative high-resolution DNA methylation analysis. *Nucleic Acids Res.* 33, 5868–5877.
- Meissner, A., Mikkelsen, T.S., Gu, H., Wernig, M., Hanna, J., Sivachenko, A., Zhang, X., Bernstein, B.E., Nusbaum, C., Jaffe, D.B., et al. (2008). Genome-scale DNA methylation maps of pluripotent and differentiated cells. *Nature* 454, 766–770.
- Okashita, N., Kumaki, Y., Ebi, K., Nishi, M., Okamoto, Y., Nakayama, M., Hashimoto, S., Nakamura, T., Sugawara, K., Kojima, N., et al. (2014). PRDM14 promotes active DNA demethylation through the ten-eleven translocation (TET)-mediated base excision repair pathway in embryonic stem cells. *Development* 141, 269–280.
- Oliveros-Etter, M., Li, Z., Nee, K., Hosohama, L., Hargan-Calvopiña, J., Lee, S.A., Joti, P., Yu, J., and Clark, A.T. (2015). PGC reversion to pluripotency involves erasure of DNA methylation from imprinting control centers followed by locus-specific re-methylation. *Stem Cell Reports* 5, 337–349.
- Ooi, S.K., Wolf, D., Hartung, O., Agarwal, S., Daley, G.Q., Goff, S.P., and Bestor, T.H. (2010). Dynamic instability of genomic methylation patterns in pluripotent stem cells. *Epigenetics Chromatin* 3, 17.
- Piccolo, F.M., Bagci, H., Brown, K.E., Landeira, D., Soza-Ried, J., Feytout, A., Mooijman, D., Hajkova, P., Leitch, H.G., Tada, T., et al. (2013). Different roles for Tet1 and Tet2 proteins in reprogramming-mediated erasure of imprints induced by EGC fusion. *Mol. Cell* 49, 1023–1033.
- Plath, K., Fang, J., Mlynarczyk-Evans, S.K., Cao, R., Worringer, K.A., Wang, H., de la Cruz, C.C., Otte, A.P., Panning, B., and Zhang, Y. (2003). Role of histone H3 lysine 27 methylation in X inactivation. *Science* 300, 131–135.
- Popp, C., Dean, W., Feng, S., Cokus, S.J., Andrews, S., Pellegrini, M., Jacobsen, S.E., and Reik, W. (2010). Genome-wide erasure of DNA methylation in mouse primordial germ cells is affected by AID deficiency. *Nature* 463, 1101–1105.
- Reik, W., and Surani, M.A. (2015). Germline and pluripotent stem cells. *Cold Spring Harb. Perspect. Biol.* 7, a019422.
- Robinson, M.D., McCarthy, D.J., and Smyth, G.K. (2010). edgeR: a Bioconductor package for differential expression analysis of digital gene expression data. *Bioinformatics* 26, 139–140.
- Schulz, E.G., Meisig, J., Nakamura, T., Okamoto, I., Sieber, A., Picard, C., Borensztein, M., Saitou, M., Blüthgen, N., and Heard, E. (2014). The two active X chromosomes in female ESCs block exit from the pluripotent state by modulating the ESC signaling network. *Cell Stem Cell* 14, 203–216.
- Sharov, A.A., Piao, Y., Matoba, R., Dudekula, D.B., Qian, Y., VanBuren, V., Falco, G., Martin, P.R., Stagg, C.A., Bassey, U.C., et al. (2003). Transcriptome analysis of mouse stem cells and early embryos. *PLoS Biol.* 1, E74.
- Sharova, L.V., Sharov, A.A., Piao, Y., Shaik, N., Sullivan, T., Stewart, C.L., Hogan, B.L.M., and Ko, M.S.H. (2007). Global gene expression profiling reveals similarities and differences among mouse pluripotent stem cells of different origins and strains. *Dev. Biol.* 307, 446–459.
- Shovlin, T.C., Durcova-Hills, G., Surani, A., and McLaren, A. (2008). Heterogeneity in imprinted methylation patterns of pluripotent embryonic germ cells derived from pre-migratory mouse germ cells. *Dev. Biol.* 313, 674–681.
- Smith, Z.D., Chan, M.M., Humm, K.C., Karnik, R., Mekhoubad, S., Regev, A., Eggan, K., and Meissner, A. (2014). DNA methylation dynamics of the human preimplantation embryo. *Nature* 511, 611–615.
- Stadtfeld, M., Maherali, N., Breault, D.T., and Hochedlinger, K. (2008). Defining molecular cornerstones during fibroblast to iPS cell reprogramming in mouse. *Cell Stem Cell* 2, 230–240.
- Tada, M., Tada, T., Lefebvre, L., Barton, S.C., and Surani, M.A. (1997). Embryonic germ cells induce epigenetic reprogramming of somatic nucleus in hybrid cells. *EMBO J.* 16, 6510–6520.
- Tada, M., Takahama, Y., Abe, K., Nakatsuji, N., and Tada, T. (2001). Nuclear reprogramming of somatic cells by in vitro hybridization with ES cells. *Curr. Biol.* 11, 1553–1558.
- Tada, T., Tada, M., Hilton, K., Barton, S.C., Sado, T., Takagi, N., and Surani, M.A. (1998). Epigenotype switching of imitable loci in embryonic germ cells. *Dev. Genes Evol.* 207, 551–561.

- Takahashi, K., and Yamanaka, S. (2006). Induction of pluripotent stem cells from mouse embryonic and adult fibroblast cultures by defined factors. *Cell* 126, 663–676.
- Takahashi, K., Mitsui, K., and Yamanaka, S. (2003). Role of ERas in promoting tumour-like properties in mouse embryonic stem cells. *Nature* 423, 541–545.
- Tyanova, S., Temu, T., Sinitcyn, P., Carlson, A., Hein, M.Y., Geiger, T., Mann, M., and Cox, J. (2016). The Perseus computational platform for comprehensive analysis of (prote)omics data. *Nat. Methods* 13, 731–740.
- von Meyenn, F., Iurlaro, M., Habibi, E., Liu, N.Q., Salehzadeh-Yazdi, A., Santos, F., Petrini, E., Milagre, I., Yu, M., Xie, Z., et al. (2016). Impairment of DNA methylation maintenance is the main cause of global demethylation in naive embryonic stem cells. *Mol. Cell* 62, 848–861.
- Yamaji, M., Ueda, J., Hayashi, K., Ohta, H., Yabuta, Y., Kurimoto, K., Nakato, R., Yamada, Y., Shirahige, K., and Saitou, M. (2013). PRDM14 ensures naive pluripotency through dual regulation of signaling and epigenetic pathways in mouse embryonic stem cells. *Cell Stem Cell* 12, 368–382.
- Yang, L., Kirby, J.E., Sunwoo, H., and Lee, J.T. (2016). Female mice lacking Xist RNA show partial dosage compensation and survive to term. *Genes Dev.* 30, 1747–1760.
- Ying, Q.-L., Wray, J., Nichols, J., Batlle-Morera, L., Doble, B., Woodgett, J., Cohen, P., and Smith, A. (2008). The ground state of embryonic stem cell self-renewal. *Nature* 453, 519–523.
- Zvetkova, I., Apedaile, A., Ramsahoye, B., Mermoud, J.E., Crompton, L.A., John, R., Feil, R., and Brockdorff, N. (2005). Global hypomethylation of the genome in XX embryonic stem cells. *Nat. Genet.* 37, 1274–1279.

STAR★METHODS

KEY RESOURCES TABLE

REAGENT or RESOURCE	SOURCE	IDENTIFIER
Antibodies		
Rabbit polyclonal anti-NANOG antibody	Abcam	Cat#ab80892; RRID:AB_2150114
Goat polyclonal anti-SOX2 antibody	Santa Cruz	Cat#c-17320
Rabbit monoclonal anti-GATA6 antibody	Cell Signaling	Cat#5851; RRID:AB_10705521
Chicken Polyclonal Anti-GFP Antibody	Novus	Cat#NB100-1614; RRID:AB_523902
Mouse monoclonal anti-OCT4 antibody	Santa Cruz	Cat#sc-5279; RRID:AB_628051
Mouse monoclonal anti-5mC antibody	Active Motif	Cat#39649
Rabbit monoclonal anti-DNMT1 antibody	Cell Signaling	Cat#5119S; RRID:AB_10545765
Rabbit polyclonal anti-DNMT3A antibody	Santa Cruz	Cat#sc-20703; RRID:AB_2093990
Mouse monoclonal anti-DNMT3B antibody	Abcam	Cat#ab13604; RRID:AB_300494
Rabbit polyclonal anti-DNMT3L antibody	Cell Signaling	Cat#12309S
Rabbit polyclonal anti-DUSP9 antibody	Abcam	Cat#ab167080
Rabbit polyclonal anti-TET2 antibody	Abcam	Cat#ab94580; RRID:AB_10887588
Rabbit monoclonal anti-phospho-ERK antibody	Cell Signaling	Cat#8544; RRID:AB_11127856
Rabbit monoclonal anti-ERK antibody	Cell Signaling	Cat#4348S; RRID:AB_10693601
Rabbit monoclonal anti-phospho-MEK antibody	Cell Signaling	Cat#9154S; RRID:AB_2138017
Mouse monoclonal anti-MEK antibody	Cell Signaling	Cat#4694S; RRID:AB_10695868
Rabbit monoclonal anti-β-ACTIN antibody	Cell Signaling	Cat#5125S; RRID:AB_1903890
Rabbit polyclonal anti-UHFR1 antibody	Santa Cruz	Cat#sc-98817; RRID:AB_2214278
Rabbit polyclonal anti-mouse serum antibody	Rockland Immunochemicals	Cat#110-4139; RRID:AB_220020
Bacterial and Virus Strains		
pLV-tetO-IRES-tdTomato	Stadfeld et al., 2008	N/A
pLV-tetO-Rhox5-GFP(Rhox5 and GFP are fused in frame)	This paper	N/A
pLV-tetO-Klf8-GFP (Klf8 and GFP are fused in frame)	This paper	N/A
pLV-tetO-Eras-IRES-tdTomato	This paper	N/A
pLV-tetO-Dusp9-IRES-tdTomato	This paper	N/A
Chemicals, Peptides, and Recombinant Proteins		
Polyethyleneglycol	Roche	Cat#10783641001
Puromycin	Thermo Scientific	Cat# A1113802
Neomycin	Sigma	Cat# N1142-20ML
Gunea-pig complement serum	Sigma	Cat#S1639-5ML
Acidic Tyrode's Solution	Millipore	Cat#MR-004-D
Advanced KSOM Embryo Medium	Millipore	Cat# MR-101-D
FLPase	Beard et al., 2006	N/A
Critical Commercial Assays		
Alkaline phosphatase staining	Vector Labs	Cat#SK-5100
EZ DNA Methylation kit	Zymo Research	Cat# D5001
Dneasy Blood & Tissue Kit	QIAGEN	Cat#69504
Streptavidin Sepharose HP	GE Healthcare Life Sciences	Cat# 17-5113-01

(Continued on next page)

Continued

REAGENT or RESOURCE	SOURCE	IDENTIFIER
PyroMark Q96 Vacuum Workstation	QIAGEN	Cat#9001528
Primer-It II Random Labeling Kit	Agilent	Cat# 300385
Deposited Data		
RNA-seq raw data	This paper	GEO: GSE94481
RRBS raw data	This paper	GEO: GSE68733
RRBS raw data for Dnmt3a/b double-knockout sample	Liao et al., 2015	GEO: GSE67811
Experimental Models: Cell Lines		
J-ESC (C57B6/6J-Tg(pPGKneobpA)3Ems/J x 129S6)	This paper	N/A
EL16.7	Lee and Lu, 1999	N/A
KH2	Beard et al., 2006	N/A
Haploid ESC (AN-312)	Elling et al., 2011	N/A
Experimental Models: Organisms/Strains		
Mouse: C57B6/6J-Tg(pPGKneobpA)3Ems/J	Jackson Laboratories	Stock # 002356
Mouse: 129S6	Taconic	Cat#129SVE-F
Mouse: X-linked GFP	Hadjantonakis et al., 2001	N/A
Mouse: B6D2F1	Jackson Laboratories	Stock # 100006
Mouse: Swiss Webster	Taconic	Cat#SW-F
Oligonucleotides		
Dusp9 sgRNA: GTCTGAGTCGGTCATGCCTG	This paper	N/A
Dusp9 KO primer F: TCAGGACAGGGGTTGA CTTC	This paper	N/A
Dusp9 KO primer R: CTGGTCGTACAGGAG CACAG	This paper	N/A
Recombinant DNA		
Mouse Dusp9 cDNA	Thermo Scientific Bio	Cat# MMM1013-202780049
Mouse Rhox5-GFP cDNA	Origene	Cat# MG202270
Mouse Klf8-GFP cDNA	Origene	Cat# MG205402
Mouse Eras cDNA	This paper	IDT ultramer was purchased
Plasmid: gRNA	Addgene (Keith Joung lab unpublished CRISPR plasmids)	Cat# 43860
Plasmid: Cas9 nuclease	Addgene (Hwang et al., 2013)	Cat#42251
Software and Algorithms		
edgeR	Robinson et al., 2010	edgeR_3.8.6.
MAQ	http://maq.sourceforge.net/	0.7.1-9
Picard pipeline	http://broadinstitute.github.io/picard/faq.html	1.623
R software suite	http://www.R-project.org	3.3.2.
Persus software	Tyanova et al., 2016	1.5.6.0.
PyroMark Q96 ID Software 2.5	QIAGEN	Cat# 9022198
GraphPad Prism 7	GraphPad	7
ImageJ	NIH	1.6.0_24.

CONTACT FOR REAGENT AND RESOURCE SHARING

Further information and requests for resources and reagents should be directed to and will be fulfilled by the Lead Contact, Konrad Hochedlinger (khochedlinger@mgh.harvard.edu).

EXPERIMENTAL MODEL AND SUBJECT DETAILS

Animal care and use

All mice used in the study were housed and bred in Specific Pathogen Free (SPF) rooms located in the AAALAC-accredited Center for Comparative Medicine vivarium at Massachusetts General Hospital. All mice were housed in ventilated cages on a standard 12:12 light cycle. All procedures involving mice adhered to the guidelines of the approved Massachusetts General Hospital Institutional Animal Care and Use Committee (IACUC) protocol no. 2006N000104. X^{GFP} mice were generated in Dr. Andras Nagy's laboratory and made available to us through Dr. Jeanie Lee's laboratory at MGH. C57B6/6J-Tg(pPGKneobpA)3Ems/J and B6D2F1 mice were obtained from Jackson labs. Swiss Webster and 129S6 mice were obtained from Taconic Biosciences.

Mouse ESC generation

E3.5 blastocysts were retrieved from the uterine horns by flushing and collected under a dissection microscope. A whole blastocyst was plated onto MEF feeders (Globalstem) containing 2i-LIF medium, which is a 1:1 mixture of DMEM/F12 and Neurobasal media (Invitrogen) supplemented with N2 (Invitrogen), B27 (Invitrogen), 1X PenStrep, 10³ IU LIF, 1 μM PD0325901 (Tocris), and 3 μM CHIR9021 (Tocris) (Ying et al., 2008). The cells were cultured for 4 days without changing medium. After that, the cells were cultured for an additional 3-4 days and fed every two days with fresh 2i-LIF medium until picking. Outgrowths from the cultures were picked, trypsinized, and re-plated onto MEF feeders in serum-LIF medium containing KO DMEM (Invitrogen) supplemented with 15% FBS (Hyclone), 1X Glutamax (GIBCO), 100 μM non-essential amino acids (GIBCO), and 0.1 mM beta-mercaptoethanol (GIBCO), 1X PenStrep (GIBCO) and 10³ IU LIF.

Mouse EGC generation

Genital ridges containing primordial germ cells (PGCs) were retrieved from E11.5/12.5 mouse embryos according to a previous protocol (Matsui et al., 1992). PGCs were collected from the genital ridges by trypsinization and centrifugation. Subsequently, isolated PGCs were cultured on stem cell factor (SCF)-secreting MEF feeders containing 2i-LIF medium as described above, and supplemented with 60 ng/ml exogenous SCF (Pepro Tech) and 10 ng/ml bFGF (Invitrogen). The cells were cultured for 3 days without changing medium. After that, the cells were cultured for additional 7-11 days and fed every other day with fresh 2i-LIF medium until picking. Outgrowth from the culture was picked, trypsinized, and re-plated onto MEF feeders containing serum-LIF medium as above.

METHODS DETAILS

Cell fusion

One million EGCs or ESCs were combined with one million MEFs in a 50 mL conical tube and then centrifuged at 1000 rpm for 5 min. After removal of the supernatant by gently decanting, the cell pellet was resuspended in the remaining medium by gently tapping the tube. 700 ul of PEG-1500 (Roche) was added in a drop-wise manner while gently stirring the tube after each drop. 10 mL of pre-warmed KO DMEM (Invitrogen) was added in a drop-wise manner at a rate of 1 mL per minute. The cells were incubated at 37°C for 5 min in the waterbath and centrifuged at 1,000 rpm for 5 min. The cell pellets were resuspended in serum-LIF medium and plated onto MEF feeders. Selection was initiated 24 hr post-fusion with puromycin (2 mg/mL) and neomycin (300 mg/mL). Cell-cycle analysis was performed on a FACSCalibur (BD) with propidium iodide; signal area was used as a measure of DNA content.

Teratoma assay

ESCs of the indicated type were grown to confluence in a single well of a confluent six well plate. Cells were then trypsinized and counted. Circa 2x10⁶ ESCs were brought up in 300 uL of ESC media and injected subcutaneously into the flank of a nu/nu immunocompromised mouse. Teratomas were monitored and removed once tumor size reached 1 cm or tumors became ulcerated, weighed, and processed for hematoxylin and eosin staining.

Blastocyst injection

Blastocyst injections were performed as previously described (Eggan et al., 2001). Briefly, female BDF1 mice were superovulated by intraperitoneal injection with 5 IU of PMSG and 48 hr later with 5 IU of hCG. Following hCG injection, the superovulated females were mated to BDF1 stud males. Zygotes were isolated from females with a vaginal plug 24 hr after hCG injection. Zygotes were cultured in vitro for 3 d in KSOM medium (Millipore), and blastocysts were injected with ESCs or EGCs and transferred into pseudopregnant recipient females.

Immunosurgery

Immunosurgery was performed as previously described (Chen and Melton, 2007). Briefly, zygotes were isolated from a cross between male mice carrying an X-linked GFP reporter (Hadjantonakis et al., 2001) and female wild-type mice. Isolated zygotes were cultured in KSOM medium (Millipore) for 4 days. E4.5 blastocysts were transferred through a series of Acidic Tyrode's Solution (Millipore) drops to dissolve the zona pellucida (usually 5-30 s) and then through a series of KSOM medium drops to rinse off Acidic Tyrode's Solution. After the removal of the zona pellucida, blastocysts were transferred through a series of drops containing Rabbit

polyclonal anti-mouse serum antibody (Rockland Immunochemicals) and left in the final drop for 30 min at 37°C. After incubation, blastocysts were transferred through a series of KSOM medium drops to rinse off primary antibody and then transferred through a series of Guinea-pig complement serum (Sigma) drops until the lysis of trophectoderm cells. The trophectoderm was removed by repetitive mouth-pipetting.

AP Staining and immunostaining

Alkaline phosphatase staining was performed using the Vector Red substrate kit (Vector Labs). Immunostaining was done according to (Plath et al., 2003). Briefly, cells/tissues were fixed with 4% paraformaldehyde for 5 min and subsequently blocked with 1% BSA, 1% donkey serum and 0.5% Triton X-100. Following blocking, cells were incubated overnight with primary antibody at 4°C. Cells were then washed 3X with PBS and incubated with secondary antibody for 1 hr at room temp. Cells/tissues were then washed 3 times with PBS, mounted, and viewed with an inverted fluorescent microscope. Antibodies used for this study were: anti-NANOG antibody (Abcam; ab80892), anti-SOX2 antibody (Santa Cruz; sc-17320), anti-GATA6 antibody (Cell signaling; #5851), anti-GFP antibody (Nobus; NB100-1614) and anti-OCT4 antibody (Santa Cruz; sc-5279).

Bisulfite Sequencing

DNA was bisulfite-converted using the EZ DNA Methylation kit (Zymo Research) and analyzed by EpigenDX using the following assays: *Peg3* (ADS183) and *Oct4* (ASY585).

Bisulfite treated DNA was purified according to the manufacturer's protocol and eluted to a final volume of 46 µL. PCRs were performed using 1 µL of bisulfite treated DNA and 0.2 µM of each primer. One primer was biotin-labeled and HPLC purified in order to purify the final PCR product using Sepharose beads. PCR product was bound to Streptavidin Sepharose HP (GE Healthcare Life Sciences), after which the immobilized PCR products were purified, washed, denatured with a 0.2 µM NaOH solution, and rewashed using the PyroMark Q96 Vacuum Workstation (QIAGEN), as per the manufacturer's protocol. Next, 0.5 µM of sequencing primer was annealed to the purified single stranded PCR products. 10 µL of the PCR products were sequenced by Pyrosequencing on the PSQ96 PyroMark System (QIAGEN) following the manufacturer's instructions.

The methylation status of each CpG site was determined individually as an artificial C/T SNP using PyroMark Q96 Advanced Software (QIAGEN). The methylation level at each CpG site was calculated as the percentage of the methylated alleles (Relative Light Unit, RLU) divided by the sum of all methylated and unmethylated alleles (RLU). The mean methylation level was calculated using methylation levels of all measured CpG sites within the targeted region of each gene. Each experiment included non-CpG cytosines as internal controls to detect incomplete bisulfite conversion of the input DNA. In addition, a series of unmethylated and methylated DNA are included as controls in each PCR. Furthermore, PCR bias testing (preferential PCR amplification of C or T allele) was performed by mixing low methylated control DNA with high methylated DNA at different ratios (0%, 5%, 10%, 25%, 50%, 75%, and 100%), followed by bisulfite modification, PCR, and Pyrosequencing analysis.

Southern blot analysis for global DNA methylation

10-15 µg of DNA was digested with Hpall and fragments were separated on a 0.8% agarose gel. The gel was rinsed in distilled water depurinated in 0.5 HCl for 25 min on a shaker and then washed in 1.5 M NaCl/0.5 M NaOH buffer for 45 min on a shaker. DNA was transferred onto HybondXL membrane (Amersham Biosciences) in transfer buffer containing 1.5 M NaCl/0.5 M NaOH overnight. The membrane was washed in 2X SCC, dried on paper towels and pre-hybridized in hybridization buffer containing 0.5 M NaPi (pH7.2), 7% SDS and 1 mM EDTA at 65°C for 3 hr in the rotator. pMR150 probe (Meissner et al., 2005) was labeled using Primer-It II Random Labeling Kit (Agilent) following the manufacturer's instructions and hybridized to the membrane in a rotating tube using a hybridization oven at 65°C overnight. The membrane was washed twice in washing buffer containing 40 mM sodium phosphate (pH7.2) and 0.1% SDS for 30 min at 65°C. The membrane was exposed to film for 24 hr or longer at room temperature before analysis.

Dot blot assay

Genomic DNA samples were diluted in TE buffer and then denatured in 0.4 M NaOH/10 mM EDTA at 95°C for 10 min and followed by adding an equal volume of cold 2 M ammonium acetate (pH 7.0). Denatured DNA samples were spotted on a nitrocellulose membrane (BIO-RAD) in an assembled Bio-Dot apparatus (BIO-Rad) according to manufacturer's instruction. The membrane was washed with 2X SSC buffer and UV-cross linked for 10 min. Then the membrane was blocked with 5% non-fat milk for 1 hr and incubated with anti-5mC (Active Motif; 39649) at 4°C overnight for HRP-conjugated secondary antibodies and enhanced chemiluminescence detection. Quantification was performed using the ImageJ software.

Reduced representation bisulfite sequencing (RRBS)

Global, base pair-resolution measurements of DNA methylation was measured by Reduced Representation Bisulfite Sequencing (RRBS) as described in (<http://genomebiology.com/2012/13/10/r92>). Briefly, genomic DNA from ESCs was digested using the Mspl enzyme which cuts at C⁺CGG sites. Bisulfite treatment of DNA fragments was used to convert unmethylated cytosines to uracil, and this change was observed after sequencing and aligning library reads to the reference genome. Libraries were sequenced using the HiSeq 2000 or HiSeq 2500 platform, and aligned to an in-silico Mspl-digested mm9 genome using MAQ (<http://maq.sourceforge.net>), or to the mm9 genome using BSMap. The Picard Pipeline (<http://broadinstitute.org.github.io/picard/faq.html>) was used for quality control.

The methylation at each covered CpG was calculated as the number of reads in which the CpG was methylated (no bisulfite conversion took place) divided by the number of total reads covering the CpG. Region analysis was performed using custom Perl scripts to summarize methylation levels at promoters (2Kb centered at refSeq transcription start sites), 1Kb tiles, and imprinting control regions as defined in (<https://www.ncbi.nlm.nih.gov/pubmed/18600261>).

RNA-sequencing

Undifferentiated EGCs/ESCs were sorted for SSEA1⁺ to control for the homogeneity of cells before RNA extraction. The quality and quantity of total input mRNA was determined on an Agilent BioAnalyzer 2100 using Agilent RNA 6000 Nano kit. One microgram of total RNA from each sample was then used as input for library preparation using Illumina TruSeq RNA Sample Prep Kit, following manufacturer's instructions. Each paired-end library was prepared with an adaptor with unique index sequence. The size profile and quantity of resulting libraries were then determined on the BioAnalyzer 2100 with Agilent High Sensitivity DNA kit. These libraries were then pooled together at equal molar concentration and sequenced on an Illumina HiSeq 2000.

RNA-seq data analysis

Unsupervised clustering for all samples was performed over expression values for genes with TPM (transcripts per million) > 1.0 in at least one of the 15 samples. For hierarchical clustering, Pearson correlation (r) between pairs of samples was computed on log(TPM+1) expression values and 1-r was used as the distance metric. Differential expression analysis was performed using the R package edgeR ([Robinson et al., 2010](#)) using the exactTest routine after normalizing read counts and excluding genes with low counts (TPM < 1.0 for 2 or more samples) ([Anders et al., 2013](#)). Differentially expressed genes were defined based on cutoffs of fold change ≥ 1.5 and FDR < 0.05 .

Western blot analysis

In order to control for the homogeneity of the cells, differentiated EGCs/ESCs were removed by pre-plating for 1 hr at 37°C. Whole cell lysates from the cells were loaded to 4%–20% gradient SDS-PAGE gels and then transferred to nitrocellulose membranes (BIO-RAD) by using Trans-Blot[®] Turbo[™] Transfer System (BIO-RAD). Blocked membranes were incubated with antibodies against the protein of interest; anti-DNMT1 (Cell Signaling; 5119S), anti-DNMT3A (Santa Cruz; sc-20703), anti-DNMT3B (Abcam; ab13604), anti-DNMT3L (Cell Signaling; 12309S), anti-DUSP9 (Abcam; ab167080), anti-UHRF1 (Santa Cruz; sc-98817), anti-NANOG (Abcam; ab80892), anti-TET2 (Abcam; ab94580) and anti- β -ACTIN (Cell Signaling; 5125S). The intensity of each band was measured using the ImageJ software and normalized to the respective loading controls.

Gene targeting of ESCs

Dusp9 cDNA was cloned into the shuttle plasmid pBS31 using NotI and MfeI digestion. The resulting plasmid was electroporated into KH2 ESCs together with a plasmid driving expression of Flp recombinase ([Beard et al., 2006](#)). Correct targeted clones were screened for by hygromycin selection and confirmed by Southern blotting as previously described ([Beard et al., 2006](#)).

Viral production

Dusp9, *RhoX5*, *Eras*, and *Klf8* cDNAs were obtained (see [Key Resources Table](#)) and cloned into tet-inducible lentiviruses ([Stadtfeld et al., 2008](#)). Lentivirus was produced by transfecting the respective plasmids into 293T cells using Polyethylenimine (PEI) along with the packaging plasmids VSV-G and Δ 8.9 in T75 flasks. Virus was collected in mES media and concentrated using an ultracentrifuge. Virus was then used to infect ESCs. After infection, the ESCs were induced with 2ug/mL of doxycycline for 72 hr, the cells were dissociated and sorted by expression of the fluorescent reporter that was cloned into the corresponding lentiviral plasmid.

Generation of *Dusp9*^{+/−} *M. musculus* x *M. castaneus* ESCs

M. musculus x *M. castaneus* hybrid female ESCs were cotransfected with a construct containing an sgRNA targeting the first exon of *Dusp9* and a Cas9 expression vector ([Hwang et al., 2013](#)) (see also [Key Resources Table](#)). Individual clones were picked, and heterozygous knockout clones were identified by PCR amplification with primers flanking the Cas9 cut site (see [Key Resources Table](#)) followed by deep sequencing to identify both alleles in each clone. Alleles containing frameshift indels (i.e., not divisible by 3) were considered to be null alleles. Expression of *Dusp9* in heterozygous clones was confirmed via western blot analysis.

X chromosome FISH

ESC lines were prepared for FISH analysis by cytogenetic direct preparation after trypsinization from cells plated on gelatin. Cells were then exposed to hypotonic solution (0.075 M KCl) for 25 min at 37°C and fixed with 3:1 methanol:acetic acid. FISH was performed using a probe for murine X chromosome (DXMit190) labeled with Red fluorochrome (ID Labs, London, Ontario, Canada) and a probe for murine Y chromosome (Whole chromosome probe) labeled with Green fluorochrome (ID Labs, London, Ontario, Canada) according to manufacturer's directions. After counterstaining with DAPI/antifade (Vectashield, Vector Laboratories, Burlingame, California), nuclei were scored for each sample by each of 2 independent scorers.

Proteomic sample preparation

Approximately 5×10^7 cells were washed twice in PBS and harvested manually using cell scrapers. The cells were centrifuged at 500 X g, flash frozen using liquid nitrogen, and stored at -80°C until lysis. Cell pellets were re-suspended in lysis buffer containing 50 mM HEPES (pH 8.5), 8 M urea, 150 mM NaCl, protease inhibitors (mini-Complete EDTA-free, Roche), and phosphatase inhibitors (PhosSTOP, Roche). Cells were then lysed via syringe lysis with 15 passes through a 22 gauge needle. Lysates were centrifuged to clear the lysate and the protein concentration was determined using a BCA assay (ThermoFisher Scientific). Equal amounts of protein (2 mg) was reduced for 45 min at 37°C with 5 mM DTT, alkylated with 15 mM IAA for 30 min at room temperature in the dark, before final reduction with 5 mM DTT for 15 min at room temperature. Protein content was then extracted through methanol-chloroform precipitation, before re-suspension in 50 mM HEPES, 8 M urea, and 150 mM NaCl. For proteolytic digestion LysC (Wako, Japan) was added at a substrate:enzyme ratio of 100:1 and incubated for 2 hr at 37°C . Samples were then diluted to 1.5 mM Urea with 50 mM HEPES before overnight digestion with Trypsin at room temperature with a substrate:enzyme ratio of 50:1. The peptide solutions were then acidified before solid-phase extraction via SepPak (Waters). Peptide samples were re-suspended in 450 μL 50% ACN, 2 M lactic acid and 100 μg of each sample was removed, desalting, and saved for protein-level measurements. Phosphopeptide enrichment was performed as previously described (Erickson et al., 2015).

Peptides saved prior to enrichment were then suspended in 100 μL of 200 mM EPPS pH 8.5 before the addition of 30 μL of anhydrous acetonitrile, and 10 μL of a 20 $\mu\text{g}/\mu\text{L}$ stock of TMT reagent. Samples were incubated for 1 hr at room temperature before the addition of 10 μL 5% hydroxylamine. A small portion of each sample was mixed, desalting, and analyzed to determine relative protein abundance in each sample. The remaining sample was then mixed to ensure equal loading of protein content and acidified before solid-phase extraction via SepPak.

Mass spectrometry analysis

Mass spectrometry analyses were performed on an Orbitrap Fusion Lumos mass spectrometer (ThermoFisher Scientific) coupled to an Easy-nLC 1200 ultra-high pressure liquid chromatography (LC) pump (ThermoFisher Scientific). Peptides were separated at 300 nL/min using a self-packed analytical column (75 μm inner diameter) that was packed with 0.5 cm of Magic C18 resin (5 μm , 100 \AA , Michrom Bioresources) followed by 35 cm of Sepax Technologies GP-C18 resin (1.8 μm , 120 \AA). LC buffers consisted of 0.1% formic acid (buffer A) and 80% ACN with 0.1% formic acid and LC gradients were optimized to ensure equal elution of peptides throughout the analysis. Intact mass analysis of peptides (MS1) was performed in the Orbitrap (AGC target 1e6, 120,000 resolution, 100 ms maximum injection time) and used to select the 10 most abundant features for MS/MS (MS2) analysis. Candidate peaks were filtered based on charge state ≥ 2 and monoisotopic peak assignment, and dynamic exclusion ($60\text{ s} \pm 7.5\text{ ppm}$) was enabled. Each precursor was isolated with using a quadrupole mass filter (0.5 Th width) and then fragmented with collision-induced dissociation (CID, 35 NCE) ion the ion trap with distinct settings for peptides (AGC target = 2.5×10^4 , maximum injection time = 200 ms). To alleviate the effects of precursor ion interference multiple fragment ions were isolated using synchronous precursor selection (SPS) prior to HCD (55 NCE, SPS notches = 8, AGC target = 2.2×10^5 , maximum injection time of 150 ms) MS3 fragmentation and Orbitrap analysis (50,000 resolution).

Mass spectrometry data analysis

A compilation of in-house software was used to convert mass spectrometric data (Thermo “.raw” files) to mzXML format, as well as to correct monoisotopic m/z measurements and erroneous peptide charge state assignments (Huttl et al., 2010). Assignment of MS/MS spectra was performed using the SEQUEST algorithm (Eng et al., 1994). Static modifications included TMT (229.16293 Da) on both the N-terminus of peptides and lysine residues and carbamidomethylation of cysteine residues (57.02146 Da). Peptide spectral matches were filtered to 1% false discovery rate (FDR) using the target-decoy strategy (Elias and Gygi, 2007), before being grouped into proteins which were then filtered to 1% FDR at the protein level as previously described (Huttl et al., 2010). Proteins isoforms were quantified as previously described (Isasa et al., 2015). “Relative abundance” expression values for protein isoform and represent the signal-to-noise value of each sample divided by the sum of all samples for each analyte normalized to 100. All data analysis was performed using R (<http://www.R-project.org>). Heatmaps and associated gene ontology enrichment were generated with Perseus (<http://www.coxdocs.org/doku.php?id=perseus:start>) (Tyanova et al., 2016).

QUANTIFICATION AND STATISTICAL ANALYSIS

Statistical parameters including the exact values of n and statistical significance are reported in the Figures and the Figure Legends. Data is judged to be statistically significant when $p < 0.05$ by two-tailed Student’s T-TEST where appropriate.

DATA AND SOFTWARE AVAILABILITY

Software

ImageJ software is available at <https://imagej.nih.gov/ij/download.html>

PyroMark Q96 Advanced Software is available at <https://www.qiagen.com/ch/shop-old/automated-solutions/pyrosequencing/pyromark-q96-id/>

edgeR software is available at <https://bioconductor.org/packages/release/bioc/html/edgeR.html>

MAQ alignment software is available at <http://maq.sourceforge.net/>
The Picard pipeline software is available at <https://github.com/broadinstitute/picard>
R software suite is available at <http://www.R-project.org>
Perseus software is available at <http://www.coxdocs.org/doku.php?id=perseus:start>

Data resources

The accession number for the raw data files for the RNA-seq analysis reported in this paper is NCBI GEO: GSE94481.
The accession number for the raw data files for the RRBS analysis reported in this paper is NCBI GEO: GSE68733.